

THE FALSE POSITIVE RATE OF *KEPLER* AND THE OCCURRENCE OF PLANETS

FRANÇOIS FRESSIN¹, GUILLERMO TORRES¹, DAVID CHARBONNEAU¹, STEPHEN T. BRYSON², JESSIE CHRISTIANSEN², COURTNEY D. DRESSING¹, JON M. JENKINS², LUCIANNE M. WALKOWICZ³, AND NATALIE M. BATALHA²

¹ Harvard-Smithsonian Center for Astrophysics, Cambridge, MA 02138, USA; ffressin@cfa.harvard.edu

² NASA Ames Research Center, Moffett Field, CA 94035, USA

³ Department of Astrophysical Sciences, Princeton University, Princeton, NJ 08544, USA

Received 2012 October 16; accepted 2012 December 15; published 2013 March 12

ABSTRACT

The *Kepler* mission is uniquely suited to study the frequencies of extrasolar planets. This goal requires knowledge of the incidence of false positives such as eclipsing binaries in the background of the targets, or physically bound to them, which can mimic the photometric signal of a transiting planet. We perform numerical simulations of the *Kepler* targets and of physical companions or stars in the background to predict the occurrence of astrophysical false positives detectable by the mission. Using real noise level estimates, we compute the number and characteristics of detectable eclipsing pairs involving main-sequence stars and non-main-sequence stars or planets, and we quantify the fraction of those that would pass the *Kepler* candidate vetting procedure. By comparing their distribution with that of the *Kepler* Objects of Interest (KOIs) detected during the first six quarters of operation of the spacecraft, we infer the false positive rate of *Kepler* and study its dependence on spectral type, candidate planet size, and orbital period. We find that the global false positive rate of *Kepler* is 9.4%, peaking for giant planets (6–22 R_{\oplus}) at 17.7%, reaching a low of 6.7% for small Neptunes (2–4 R_{\oplus}), and increasing again for Earth-size planets (0.8–1.25 R_{\oplus}) to 12.3%. Most importantly, we also quantify and characterize the distribution and rate of occurrence of planets down to Earth size with no prior assumptions on their frequency, by subtracting from the population of actual *Kepler* candidates our simulated population of astrophysical false positives. We find that $16.5\% \pm 3.6\%$ of main-sequence FGK stars have at least one planet between 0.8 and 1.25 R_{\oplus} with orbital periods up to 85 days. This result is a significant step toward the determination of eta-earth, the occurrence of Earth-like planets in the habitable zone of their parent stars. There is no significant dependence of the rates of planet occurrence between 0.8 and 4 Earth radii with spectral type. In the process, we also derive a prescription for the signal recovery rate of *Kepler* that enables a good match to both the KOI size and orbital period distribution, as well as their signal-to-noise distribution.

Key words: binaries: eclipsing – methods: data analysis – methods: statistical – planetary systems

Online-only material: color figures

1. INTRODUCTION

In 2011 February, the *Kepler* mission produced a catalog of more than 1200 candidate transiting planets, referred to as *Kepler* Objects of Interest (KOIs). These candidates were identified during the first four months of operation of the spacecraft (Borucki et al. 2011) in its quest to determine the frequency of Earth-size planets around Sun-like stars. This unprecedented sample of potential exoplanets has become an invaluable resource for all manner of statistical investigations of the properties and distributions of planets around main-sequence stars. The most recent *Kepler* release expanded the sample to more than 2300 candidates (Batalha et al. 2013), based on 16 months of observation. The analysis of this information must contend, however, with the fact that not all photometric signals are caused by planets. Indeed, false positive contamination is typically the main concern in transit surveys (see, e.g., Brown 2003), including *Kepler*, because there is a large array of astrophysical phenomena that can produce small periodic dimmings in the light of a star that can be virtually indistinguishable from those due to a true planetary transit. A common example is a background eclipsing binary falling within the photometric aperture of a *Kepler* target.

Many of the most interesting candidate transiting planets identified by the *Kepler* mission cannot be confirmed with current spectroscopic capabilities, that is, by the detection of the reflex motion of the star due to the gravitational pull from the planet. Included in this category are essentially all Earth-size

planets, as well as most super-Earths that are in the habitable zone of Sun-like stars, which have Doppler signals too small to detect. Faced with this difficulty, the approach adopted for such objects is statistical in nature and consists in demonstrating that the likelihood of a planet is much greater than that of a false positive, a process referred to as “validation.” The *Kepler* team has made extensive use of a technique referred to as BLENDER (Torres et al. 2004, 2011; Fressin et al. 2011) to validate a number of KOIs, including the majority of the smallest known exoplanets discovered to date. This technique requires an accurate knowledge of the target star usually derived from spectroscopy or asteroseismology, and makes use of other follow-up observations for the candidate including high spatial resolution imaging, *Spitzer* observations when available, and high-resolution spectroscopy. The telescope facilities required to gather such observations are typically scarce, so it is generally not possible to have these constraints for thousands of KOIs such as those in the recent list by Batalha et al. (2013). For this reason, the *Kepler* team has concentrated the BLENDER efforts only on the most interesting and challenging cases.

Based on the previous list of *Kepler* candidates by Borucki et al. (2011) available to them, Morton & Johnson (2011, hereafter MJ11) investigated the false positive rate for KOIs, and its dependence on some of the candidate-specific properties, such as brightness and transit depth. They concluded that the false positive rate is smaller than 10% for most of the KOIs, and less than 5% for more than half of them. This conclusion differs significantly from the experience of all previous transit surveys,

where the rates were typically up to an order of magnitude larger (e.g., $\sim 80\%$ for the HATNet survey; Latham et al. 2009). The realization that the *Kepler* rate is much lower than for the ground-based surveys allowed the community to proceed with statistical studies based on lists of mere *candidates*, without too much concern that false positive contamination might bias the results (e.g., Howard et al. 2012).

In their analysis, MJ11 made a number of simplifying assumptions that allowed them to provide these first estimates of the false positive rate for *Kepler*, but that are possibly not quite realistic enough for the most interesting smaller signals with lower signal-to-noise ratios (S/Ns). A first motivation for the present work is thus to improve upon those assumptions and at the same time to approach the problem of false positive rate determination in a global way, by numerically simulating the population of blends in greater detail for the entire sample of *Kepler* targets. A second motivation of this paper is to use our improved estimates of the false positive rate to extract the true frequencies of planets of different sizes (down to Earth size) as well as their distributions in terms of host star spectral types and orbital characteristics, a goal to which the *Kepler* mission is especially suited to contribute.

Regarding our first objective—the determination of the false positive rate of *Kepler*—the assumptions by MJ11 we see as potentially having the greatest impact on their results are the following.

1. The MJ11 false positive rate is based on an assumed 20% planet occurrence, with a power-law distribution of planet sizes between 0.5 and 20 R_{\oplus} (peaking at small planets) independently of the orbital period or stellar host characteristics. This is a rather critical hypothesis, as the frequency of the shortest- or longest-period objects in the KOI sample is essentially unknown. The adoption of a given planet frequency to infer the false positive rate in poorly understood regions of parameter space is risky, and may constitute circular reasoning.
2. The scenarios MJ11 included as possible blends feature both background eclipsing binaries and eclipsing binaries physically associated with the target. However, other configurations that can also mimic transit signals were not considered, such as those involving larger planets transiting an unseen physical companion or a background star. These configurations are more difficult to rule out with follow-up observations, and BLENDER studies have shown that such scenarios are often the most common blend configuration for candidates that have been carefully vetted (see, e.g., Batalha et al. 2011; Cochran et al. 2011; Ballard et al. 2011; Fressin et al. 2012a; Gautier et al. 2012; Borucki et al. 2012).
3. A key ingredient in the MJ11 study is the strong constraint offered by the analysis of the motion of the centroid of the target in and out of transit based on the *Kepler* images themselves, which can exclude all chance alignments with background eclipsing binaries beyond a certain angular separation. They adopted for this angular separation a standard value of $2''$ based on the single example of Kepler-10 b (Batalha et al. 2011), and then scaled this result for other KOIs assuming certain intuitive dependencies with target brightness and transit depth. As it turns out, those dependencies are not borne out by actual multi-quarter centroid analyses performed since, and reported by Batalha et al. (2013).

4. MJ11 did not consider the question of detectability of both planets and false positives, and its dependence on the noise level for each *Kepler* target star as well as on the period and duration of the transit signals.
5. The overall frequency and distribution of eclipsing binaries in the *Kepler* field, which enters the calculation of the frequency of background blends, has been measured directly by the *Kepler* mission itself (Prša et al. 2011; Slawson et al. 2011), and is likely more accurate at predicting the occurrence of eclipsing binaries in the solar neighborhood than inferences from the survey of non-eclipsing binary stars by Raghavan et al. (2010), used by MJ11.

The above details have the potential to bias the estimates of the false positive rate by factors of several, especially for the smaller candidates with low S/Ns. Indeed, recent observational evidence suggests the false positive rate may be considerably higher than claimed by MJ11. In one example, Demory & Seager (2011) reported that a significant fraction (14%) of the 115 hot Jupiter candidates they examined, with radii in the 8–22 R_{\oplus} range, show secondary eclipses inconsistent with the planetary interpretation. The false positive rate implied by the MJ11 results for the same radius range is only 4%. Santerne et al. (2012) recently conducted an extensive spectroscopic follow-up campaign using the HARPS and SOPHIE spectrographs, and observed a number of hot Jupiters with periods under 25 days, transit depths greater than 0.4%, and host star magnitudes $K_p < 14.7$ in the *Kepler* bandpass. They reported finding a false positive rate of $34.8\% \pm 6.5\%$. In contrast, the MJ11 results imply an average value of 2.7% for the same period, depth, and magnitude ranges, which is a full order of magnitude smaller.

We point out that Morton (2012) recently published an automated validation procedure for exoplanet transit candidates based on a similar approach as the MJ11 work, with the improvement that it now considers background stars transited by planets as an additional source of potential blends (item 2 above). However, the Morton (2012) work does not quantify the global false positive rate of *Kepler*, but focuses instead on false alarm probabilities for individual transit candidates. The methodology makes use of candidate-specific information such as the transit shape that was not explicitly considered in the actual vetting procedure used by the *Kepler* team to generate the KOI list. Here, we have chosen to emulate the *Kepler* procedures to the extent possible so that we may make a consistent use of the KOI list as published.

Regarding the second goal of our work—to determine the rate of occurrence of planets of different sizes—a main concern that such statistical studies must necessarily deal with is the issue of detectability. Only a fraction of the planets with the smallest sizes and the longest periods have passed the detection threshold of *Kepler*. The studies of Catanzarite & Shao (2011) and Traub (2012), based on the KOI catalog of Borucki et al. (2011), assumed the sample of Neptune-size and Jupiter-size planets to be both complete (i.e., that all transiting planets have been detected by *Kepler*) and essentially free of contamination (i.e., with a negligible false positive rate). They then extrapolated to infer the occurrence rate of Earth-size planets assuming it follows the occurrence versus size trend of larger planets. The more detailed study of Howard et al. (2012) focused on the sub-sample of KOIs for which *Kepler* is closer to completeness, considering only planets larger than 2 R_{\oplus} and with periods shorter than 50 days. They tackled the issue of detectability by making use of the Combined Differential Photometric Precision

(CDPP) estimates for each KOI to determine the completeness of the sample. The CDPP is designed to be an estimator of the noise level of *Kepler* light curves on the timescale of planetary transits, and is available for each star *Kepler* has observed. Howard et al. (2012) found a rapid increase in planet occurrence with decreasing planet size that agrees with the predictions of the core-accretion formation scenario, but disagrees with population synthesis models that predict a dearth of objects with super-Earth and Neptune sizes for close-in orbits. They also reported that the occurrence of planets between 2 and 4 R_{\oplus} in the *Kepler* field increases linearly with decreasing effective temperature of the host star. Their results rely to some degree on the conclusions of MJ11 regarding the rate of false positives of the sub-sample of KOIs they studied, and it is unclear how the issues enumerated above might affect them. In an independent study, Youdin (2011) developed a method to infer the underlying planetary distribution from that of the *Kepler* candidates published by Borucki et al. (2011). He investigated the occurrence of planets down to 0.5 R_{\oplus} , but without considering false positives, and relied on the simplified *Kepler* detection efficiency model from Howard et al. (2012). He reported a significant difference in the size distributions of shorter- ($P < 7$ days) and longer-period planets.

Aside from the question of detectability, we emphasize that the occurrence rate of Earth-size planets is still effectively unknown. *Kepler* is the only survey that has produced a list of Earth-size planet *candidates*, and because of the issues raised above, strictly speaking we cannot yet rule out that the false positive rate is much higher for such challenging objects than it is for larger ones, even as high as 90%. Indeed, MJ11 predicted false positive rates with the *assumption* of an overall 20% planet frequency, peaking precisely for the smallest planets. The question of the exact rate of occurrence of small planets has implications for other conclusions from *Kepler*. For example, Lissauer et al. (2012) have recently shown that most KOIs with multiple candidates (“multis”) are bona fide planets. However, if Earth-size planets are in fact rare, then most multis involving Earth-size candidates would likely correspond to *larger* objects transiting (together) the same unseen star in the photometric aperture of the target, rather than being systems comprised of true Earth-size planets.

Our two objectives, the determination of the false positive rate for *Kepler* and the determination of the occurrence rate of planets in different size ranges, are in fact interdependent, as described below. We have organized the paper as follows. In Section 2, we summarize the general approach we follow. The details of how we simulate false positives and quantify their frequency are given in Section 3, separately for each type of blend scenario including background or physically associated stars eclipsed by another star or by a planet. At the end of this section, we provide an example of the calculation for one of those scenarios. Section 4 is a summary of the false positive rates for planets of different sizes in the *Kepler* sample as a whole. In Section 5, we describe the study of the *Kepler* detection rate, and how we estimate the frequencies of planets. We derive the occurrence of planets in different size ranges in Section 6, where we examine also the dependence of the frequencies on the spectral type (mass) of the host star and other properties. In Section 7, we study the distribution of the transit durations of our simulated planet population. We discuss the assumptions and possible improvements of our study in Section 8, and conclude by listing our main results in Section 9. Finally, an Appendix describes how we model the detection process of *Kepler* and how

we infer the exclusion limit from the centroid motion analysis for each individual target.

2. GENERAL APPROACH

2.1. False Positive Simulation

The first part of our analysis is the calculation of the false positive rate for *Kepler* targets. We consider here all *Kepler* targets that have been observed in at least one out of the first six quarters of operation of the spacecraft (Q1–Q6),⁴ to be consistent with the selection imposed on the Batalha et al. (2013) list, which comes to a total of 156,453 stars. For each of these stars, identified by a unique *Kepler* Input Catalog (KIC) number (Brown et al. 2011), we have available their estimated mass, surface gravity $\log g$, and brightness in the *Kepler* bandpass (Kp magnitude) as listed in the KIC.⁵ Additionally, we have their CDPP values on different timescales and for different quarters, provided in the Mikulski Archive for Space Telescopes (MAST) at STScI.⁶ The CDPP allows us to estimate the detectability of each type of false positive scenario.

We perform Monte Carlo simulations specific to each *Kepler* target to compute the number of blends of different kinds that we expect. The calculations are based on realistic assumptions about the properties of objects acting as blends, informed estimates about the frequencies of such objects either in the background or physically associated with the target, the detectability of the signals produced by these blends for the particular star in question based on its CDPP, and also on the ability to reject blends based on constraints provided by the centroid motion analysis or the presence of significant secondary eclipses. Blended stars beyond a certain angular distance from the target can be detected in the standard vetting procedures carried out by the *Kepler* team because they cause changes in the flux-weighted centroid position, depending on the properties of the signal. This constraint, and how we estimate it for each star, is described more fully in the Appendix. The inclusion of detectability and the constraint from centroid motion analysis are included in order to emulate the vetting process of *Kepler* to a reasonable degree.

2.2. Planet Occurrence Simulation

The second part of our analysis seeks to determine the rate of occurrence of planets of different sizes. For this we compare the frequencies and distributions of simulated false positive from the previous step with those of the real sample of KOIs given by Batalha et al. (2013). We interpret the differences between these two distributions as due to true detectable planets. In order to obtain the actual rate of occurrence of planets, it is necessary to correct for the fact that the KOI list includes only planets with orbital orientations such that they transit, and for the fact that some fraction of transiting planets are not detectable by *Kepler*. We determine these corrections by means of Monte Carlo simulations of planets orbiting the *Kepler* targets, assuming initial distributions of planets as a function of planet size and orbital period (Howard et al. 2012). We then compare our simulated population of detectable transiting planets with that of KOIs minus our simulated false positive population, and we

⁴ A quarter corresponds to a period of observation of about three months between 90° spacecraft rolls designed to keep the solar panels properly illuminated.

⁵ A number of biases are known to exist in the properties listed in the KIC, the implications of which will be discussed later in Section 8.

⁶ <http://stdatu.stsci.edu/kepler/>

adjust our initial assumptions for the planetary distributions. We proceed iteratively to obtain the occurrence of planets that provides the best match to the KOI list. This analysis permits us to also study the dependence of the occurrence rates on properties such as the stellar mass.

For the purpose of interpreting both the false positive rates and the frequencies of planets, we have chosen to separate planets into five different size (radius R_p) ranges.

1. Giant planets: $6 R_{\oplus} < R_p \leq 22 R_{\oplus}$.
2. Large Neptunes: $4 R_{\oplus} < R_p \leq 6 R_{\oplus}$.
3. Small Neptunes: $2 R_{\oplus} < R_p \leq 4 R_{\oplus}$.
4. Super-Earths: $1.25 R_{\oplus} < R_p \leq 2 R_{\oplus}$.
5. Earths: $0.8 R_{\oplus} < R_p \leq 1.25 R_{\oplus}$.

An astrophysical false positive that is not ruled out by centroid motion analysis and that would produce a signal detectable by *Kepler* with a transit depth corresponding to a planet in any of the above categories is counted as a viable blend, able to mimic a true planet in that size range. These five classes were selected as a compromise between the number of KOIs in each group and the nomenclature proposed by the *Kepler* team (Borucki et al. 2011; Batalha et al. 2013). In particular, we have subdivided the 2–6 R_{\oplus} category used by the *Kepler* team into “small Neptunes” and “large Neptunes.” Howard et al. (2012) chose the same separation in their recent statistical study of the frequencies of planets larger than 2 R_{\oplus} , in which they claimed that the smallest planets (small Neptunes) are more common among later-type stars, but did not find the same trend for larger planets. Our detailed modeling of the planet detectability for each KOI, along with our new estimates of the false positive rates among small planets, enables us to extend the study to two smaller classes of planets, and to investigate whether the claims by Howard et al. (2012) hold for objects as small as the Earth.

3. FALSE POSITIVES

There exists a wide diversity of astrophysical phenomena that can lead to periodic dimming in the light curve of a *Kepler* target star and might be interpreted as a signal from a transiting planet. These phenomena involve other stars that fall within the photometric aperture of the target and contribute light. One possibility is a background star (either main-sequence or giant) eclipsed by a smaller object; another is a main-sequence star physically associated with the target and eclipsed by a smaller object. In both cases, the eclipsing body may be either a smaller star or a planet. There are thus four main categories of false positives, which we consider separately below. We also discuss the possibility that the eclipsing objects may be brown dwarfs or white dwarfs.

We make here the initial assumption that all KOIs that have passed the nominal detection threshold of *Kepler* are due to astrophysical causes, as opposed to instrumental causes such as statistical noise or aliases from transient events in the *Kepler* light curve. The expected detection rate (D_r) based on a matched filter method used in the *Kepler* pipeline is discussed by Jenkins et al. (1996). It is given by the following formula, as a function of the S/N of the signal and a certain threshold, assuming that the (possibly non-white) observational noise is Gaussian:

$$D_r(S/N) = 0.5 + 0.5 \operatorname{erf}[(S/N - 7.1)/\sqrt{2}]. \quad (1)$$

In this expression erf is the standard error function, and the adopted 7.1 σ threshold was chosen so that no more than one false positive will occur over the course of the mission due

to random fluctuations (see Jenkins et al. 2010a). The formula corresponds to the cumulative probability density function of a zero mean, unit variance Gaussian variable, evaluated at a point representing the distance between the threshold and the S/N. The construction of the matched filter used in the *Kepler* pipeline is designed to yield detection statistics drawn from this distribution. With this in mind, only 50% of transits with an S/N of 7.1 will be detected. The detection rates are 2.3%, 15.9%, 84.1%, 97.7%, and 99.9% for S/Ns of 5.1, 6.1, 8.1, 9.1, and 10.1. Below in Section 5.1, we will improve upon this initial detection model, but we proceed for now with this prescription for clarity.

Our simulation of the vetting process carried out by the *Kepler* team includes two tests that the astrophysical scenarios listed above must pass in order to be considered viable false positives (that could be considered a planet candidate): the most important is that they must not produce a detectable shift in the flux centroid. Additionally, for blends involving eclipsing binaries, they must not lead to secondary eclipses that are of similar depth as the primary eclipses (within 3σ).

3.1. Background Eclipsing Binaries

We begin by simulating the most obvious type of false positive involving a background (or foreground) eclipsing binary in the photometric aperture of the target star, whose eclipses are attenuated by the light of the target and reduced to a shallow transit-like event. We model the stellar background of each of the 156,453 KIC targets using the Besançon model of the Galaxy (Robin et al. 2003).⁷ We simulate 1 deg² areas at the center of each of the 21 modules comprising the focal plane of *Kepler* (each module containing two CCDs), and record all stars (of any luminosity class) down to 27th magnitude in the *R* band, which is sufficiently close to *Kepler*’s *Kp* band for our purposes. This limit of $R = 27$ corresponds to the faintest eclipsing binary that can mimic a transit by an Earth-size planet, after dilution by the target. We assign to each *Kepler* target a background star drawn randomly from the simulated area for the module it is located on, and we assign also a coefficient N_{bs} to represent the average number of background stars down to 27th magnitude in the 1 deg² region around the target.

Only a fraction of these background stars will be eclipsing binaries, and we take this fraction from results of the *Kepler* mission itself, reported in the work of Slawson et al. (2011). The catalog compiled by these authors provides not only the overall rate of occurrence of eclipsing binaries (1.4%, defined as the number of eclipsing binaries found by *Kepler* divided by the number of *Kepler* targets), but also their eclipse depth and period distributions. In practice, we adopt a somewhat reduced frequency of eclipsing binaries $F_{eb} = 0.79\%$ that excludes contact systems, as these generally cannot mimic a true planetary transit because the flux varies almost continuously throughout the orbital cycle. We consider only detached, semi-detached, and unclassified eclipsing binaries from the Slawson et al. (2011) catalog. Furthermore, we apply two additional corrections to this overall frequency that depend on the properties of the background star. The first factor, C_{bf} , adjusts the eclipsing binary frequency according to spectral type, as earlier-type stars have been found to have a significantly higher binary frequency than later-type stars. We interpolate this correction from Figure 12 of Raghavan et al. (2010). The second factor, C_{geom} , accounts for

⁷ The accuracy of the stellar densities (number of stars per square degree) per magnitude bin provided by this model has been tested against actual star counts at the center of the *Kepler* field. The results have been found to be consistent within 15% (R. Gilliland 2010, private communication).

the increased chance that a larger star in the background would be eclipsed by a companion of a given period, from geometrical considerations. This correction factor is unity for a star of $1 R_{\odot}$, and increases linearly with radius. We note that the scaling law we have chosen does not significantly impact the overall occurrence of eclipsing binaries established by Slawson et al. (2011), as the median radius of a *Kepler* target ($0.988 R_{\odot}$) is very close to $1 R_{\odot}$. The size of each of our simulated background stars is provided by the Besançon model.

Next, we assign a companion star to each of the 156,453 background stars drawn from the Besançon model, with properties (eclipse depth and orbital period) taken randomly from the Slawson et al. (2011) catalog. We then check whether the transit-like signal produced by this companion has the proper depth to mimic a planet with a radius in the size category under consideration (Section 2.2), after dilution by the light of the *Kepler* target (which depends on the known brightness of the target and of the background star). If it does not, we reject it as a possible blend. Next we compute the S/N of the signal as described in the Appendix, and we determine whether this false positive would be detectable by the *Kepler* pipeline as follows. For each KIC target observed by *Kepler* between Q1 and Q6 we compute the S/N as explained in the Appendix, and with Equation (1) we derive D_r . We then draw a random number between 0 and 1 and compare it with D_r ; if larger, we consider the false positive signal to be detectable. We also estimate the fraction of the N_{bs} stars that would be missed in the vetting carried out by the *Kepler* team because they do not induce a measurable centroid motion. This contribution, F_{cent} , is simply the fraction of background stars interior to the exclusion limit set by the centroid analysis. As we describe in more detail in the Appendix, the size of this exclusion region is itself mainly a function of the S/N.

Based on all of the above, we compute the number N_{beb} of background (or foreground) eclipsing binaries in the *Kepler* field that could mimic the signal of a transiting planet in a given size range as

$$N_{beb} = \sum_{i=1}^{N_{targ}} N_{bs} F_{eb} C_{bf} C_{geom} T_{depth} T_{det} T_{sec} F_{cent},$$

where F terms represent fractions, C terms represent corrections to the eclipsing binary frequency, and T terms are either 0 or 1.

1. N_{targ} is the number of *Kepler* targets observed for at least one quarter during the Q1–Q6 observing interval considered here.
2. N_{bs} is the average number of background stars down to magnitude $R = 27$ in a 1 deg^2 area around the target star.
3. F_{eb} is the frequency of eclipsing binaries, defined as the fraction of eclipsing binaries (excluding contact systems) found by *Kepler* divided by the number of *Kepler* targets, and is 0.79% for this work.
4. C_{bf} is a correction to the binary occurrence rate F_{eb} that accounts for the dependence on stellar mass (or spectral type), following Raghavan et al. (2010).
5. C_{geom} is a correction to the geometric probability of eclipse that takes into account the dependence on the size of the background star.
6. T_{depth} is 1 if the signal produced by the background eclipsing binary has a depth corresponding to a planet in the size range under consideration, after accounting for dilution by the *Kepler* target, or 0 otherwise.

7. T_{det} is 1 if the signal produced by the background eclipsing binary is detectable by the *Kepler* pipeline, or 0 otherwise.
8. T_{sec} is 1 if the background eclipsing binary does not show a secondary eclipse detectable by the *Kepler* pipeline, or 0 otherwise. We note that we have also set T_{sec} to 1 if the simulated secondary eclipses have a depth within 3σ of that of the primary eclipse, as this could potentially be accepted by the pipeline as a transiting object, with a period that is half of the binary period.
9. F_{cent} is the fraction of the N_{bs} background stars that would show no significant centroid shifts, i.e., that are interior to the angular exclusion region that is estimated for each star, as explained in the Appendix.

3.2. Background Stars Transited by Planets

A second type of astrophysical scenario that can reproduce the shape of a small transiting planet consists of a larger planet transiting a star in the background (or foreground) of the *Kepler* target. We proceed in a similar way as for background eclipsing binaries, except that instead of assigning a stellar companion to each background star, we assign a random planetary companion drawn from the actual list of KOIs by Batalha et al. (2013). However, there are three factors that prevent us from using this list as an unbiased sample of transiting planets: (1) the list is incomplete, as the shallowest and longest period signals are only detectable among the *Kepler* targets in the most favorable cases; (2) the list contains an undetermined number of false positives; and (3) the occurrence of planets of different sizes may be correlated with the spectral type of the host star (see Howard et al. 2012).

While it is fairly straightforward to quantify the incompleteness by modeling the detectability of signals for the individual KOIs (see the Appendix for a description of the detection model we use), the biases (2) and (3) are more difficult to estimate. We adopt a bootstrap approach in which we first determine the false positive rate and the frequencies for the larger planets among the KOIs, and we then proceed to study successively smaller planets. The only false positive sources for the larger planet candidates involve even larger (that is, stellar) objects, for which the frequency and distributions of the periods and eclipse depths are well known (i.e., from the work of Slawson et al. 2011). Comparing the population of large-planet KOIs (of the “giant planet” class previously defined) to the one of simulated false positives that can mimic their signals enables us to obtain the false positive correction factor (2). This, in turn, allows us to investigate whether the frequency of large planets is correlated with spectral type (see Section 6), and therefore to address bias (3) above. As larger planets transiting background stars are potential false positive sources for smaller planets, once we have understood the giant planet population we may proceed to estimate the false positive rates and occurrence of each of the smaller planet classes in order of decreasing size, applying corrections for the biases in the same way as described above.

We express the number N_{btp} of background stars in the *Kepler* field with larger transiting planets able to mimic the signal of a true transiting planet in a given size class as

$$N_{btp} = \sum_{i=1}^{N_{targ}} N_{bs} F_{tp} C_{tpf} C_{geom} T_{depth} T_{det} F_{cent},$$

where N_{targ} , N_{bs} , C_{geom} , T_{depth} , T_{det} , and F_{cent} have similar meanings as before, and

1. F_{tp} is the frequency of transiting planets in the size class under consideration, computed as the fraction of suitable KOIs found by *Kepler* divided by the number of non-giant *Kepler* targets (defined as those with KIC values of $\log g > 3.6$, following Brown et al. 2011)⁸;
2. C_{tpf} is a correction factor to the transiting planet frequency F_{tp} that accounts for the three biases mentioned above: incompleteness, the false positive rate among the KOIs of Batalha et al. (2013), and the potential dependence of F_{tp} on the spectral type of the background star.

3.3. Companion Eclipsing Binaries

An eclipsing binary gravitationally bound to the target star (forming a hierarchical triple system) may also mimic a transiting planet signal since its eclipses can be greatly attenuated by the light of the target. The treatment of this case is somewhat different from the one of background binaries, though, as the occurrence rate of intruding stars eclipsed by others is independent of the Galactic stellar population. To simulate these scenarios, we require knowledge of the frequency of triple systems, which we adopt from the results of a volume-limited survey of the multiplicity of solar-type stars by Raghavan et al. (2010). They found that 8% of their sample stars are triples, and another 3% have higher multiplicity. We therefore adopt a total frequency of $8\% + 3\% = 11\%$, since additional components beyond three merely produce extra dilution, which is small in any case compared to that of the *Kepler* target itself (assumed to be the brighter star). Of all possible triple configurations, we consider only those in which the tertiary star eclipses the close secondary, with the primary star being farther removed (hierarchical structure). The two other configurations involving a secondary star eclipsing the primary or the tertiary eclipsing the primary would typically not result in the target being promoted to a KOI, as the eclipses would be either very deep or “V”-shaped. Thus, we adopt one-third of 11% as the relevant frequency of triple- and higher-multiplicity systems.

We proceed to simulate this type of false positive by assigning to each *Kepler* target a companion star (“secondary”) with a random mass ratio q (relative to the target), eccentricity e , and orbital period P drawn from the distributions presented by Raghavan et al. (2010), which are uniform in q and e , and lognormal in P . We further infer the radius and brightness of the secondary in the Kp band from a representative 3 Gyr solar-metallicity isochrone from the Padova series of Girardi et al. (2000). We then assign to each of these secondaries an eclipsing companion, with properties (period and eclipse depth) taken from the catalog of *Kepler* eclipsing binaries by Slawson et al. (2011), as we did for background eclipsing binaries in Section 3.1. We additionally assign a mass ratio and eccentricity to the tertiary from the above distributions.

To determine whether each of these simulated triple configurations constitutes a viable blend, we perform the following four tests: (1) we check whether the triple system would be dynamically stable, to first order, using the condition for stability given by Holman & Wiegert (1999); (2) we check whether the resulting depth of the eclipse, after accounting for the light of the target, corresponds to the depth of a transiting planet in the size range under consideration; (3) we determine whether the transit-like signal would be detectable, with the same signal-to-noise criterion used earlier; and (4) we check whether the

eclipsing binary would be angularly separated enough from the target to induce a centroid shift. For this last test, we assign a random orbital phase to the secondary in its orbit around the target, along with a random inclination angle from an isotropic distribution, a random longitude of periastron from a uniform distribution, and a random eccentricity drawn from the distribution reported by Raghavan et al. (2010). The semimajor axis is a function of the known masses and the orbital period. The final ingredient is the distance to the system, which we compute using the apparent magnitude of the *Kepler* target as listed in the KIC and the absolute magnitudes of the three stars from the Padova isochrone, ignoring extinction. If the resulting angular separation is smaller than the radius of the exclusion region from centroid motion analysis, we count this as a viable blend.

The number N_{ceb} of companion eclipsing binary configurations in the *Kepler* field that could mimic the signal of a transiting planet in each size category is given by

$$N_{\text{ceb}} = \sum_{i=1}^{N_{\text{targ}}} F_{\text{eb/triple}} C_{\text{geom}} T_{\text{stab}} T_{\text{depth}} T_{\text{det}} T_{\text{sec}} T_{\text{cent}},$$

in which N_{targ} , C_{geom} , T_{depth} , T_{sec} , and T_{det} represent the same quantities as in previous sections, while

1. $F_{\text{eb/triple}}$ is the frequency of eclipsing binaries in triple systems (or systems of higher multiplicity) in which the secondary star is eclipsed by the tertiary. As indicated earlier, we adopt a frequency of eclipsing binaries in the solar neighborhood of $F_{\text{eb}} = 0.79\%$, from the *Kepler* catalog by Slawson et al. (2011). The frequency of stars in binaries and higher-multiplicity systems has been given by Raghavan et al. (2010) as $F_{\text{bin}} = 44\%$ (where we use the notation “bin” to mean “non-single”). Therefore, the chance of a random pair of stars to be eclipsing is $F_{\text{eb}}/F_{\text{bin}} = 0.0079/0.44 = 0.018$. As mentioned earlier, we will assume here that one-third of the triple star configurations (with a frequency F_{triple} of 11%, according to Raghavan et al. 2010) have the secondary and tertiary as the close pair of the hierarchical system. $F_{\text{eb/triple}}$ is then equal to $F_{\text{eb}}/F_{\text{bin}} \times 1/3 \times F_{\text{triple}} = 0.018 \times 1/3 \times 0.11 = 0.00066$. The two other configurations in which the secondary or tertiary is eclipsing the primary would merely correspond to target binaries slightly diluted by the light of a companion, and we assume here that those configurations would not have passed the *Kepler* vetting procedure.
2. T_{stab} is 1 if the triple system is dynamically stable, and 0 otherwise.
3. T_{cent} is 1 if the triple system does not induce a significant centroid motion, and 0 otherwise.

3.4. Companion Transiting Planets

Planets transiting a physical stellar companion to a *Kepler* target can also produce a signal that will mimic that of a smaller planet around the target itself. One possible point of view regarding these scenarios is to *not* consider them a false positive, as a planet is still present in the system, only not of the size anticipated from the depth of the transit signal. However, since one of the goals of the present work is to quantify the rate of occurrence of planets in specific size categories, a configuration of this kind would lead to the incorrect classification of the object as belonging to a smaller planet class, biasing the rates of occurrence. For this reason, we consider these scenarios to be a legitimate false positive.

⁸ We do not consider background giant stars transited by a planet as a viable blend, as the signal would likely be undetectable.

To quantify them we proceed in a similar way as for companion eclipsing binaries in the preceding section, assigning a bound stellar companion to each target in accordance with the frequency and known distributions of binary properties from Raghavan et al. (2010), and assigning a transiting planet to this bound companion using the KOI list by Batalha et al. (2013). Corrections to the rates of occurrence F_{tp} are as described in Section 3.2. The total number of false positives of this kind among the *Kepler* targets is then

$$N_{\text{ctp}} = \sum_{i=1}^{N_{\text{targ}}} F_{\text{bin}} F_{\text{tp}} C_{\text{geom}} C_{\text{tpf}} T_{\text{depth}} T_{\text{det}} T_{\text{cent}} T_{\text{stab}},$$

where F_{bin} is the frequency of non-single stars in the solar neighborhood (44%; Raghavan et al. 2010) and the remaining symbols have the same meaning as before.

Adding up the contributions from this section and the preceding three, the total number of false positives in the *Kepler* field due to physically bound or background/foreground stars eclipsed by a smaller star or by a planet is $N_{\text{beb}} + N_{\text{btp}} + N_{\text{ceb}} + N_{\text{ctp}}$.

3.5. Eclipsing Pairs Involving Brown Dwarfs and White Dwarfs

Because of their small size, brown dwarfs transiting a star can produce signals that are very similar to those of giant planets. Therefore, they constitute a potential source of false positives, not only when directly orbiting the target but also when eclipsing a star blended with the target (physically associated or not). However, because of their larger mass and non-negligible luminosity, other evidence would normally betray the presence of a brown dwarf, such as ellipsoidal variations in the light curve (for short periods), secondary eclipses, or even measurable velocity variations induced on the target star. Previous Doppler searches have shown that the population of brown dwarf companions to solar-type stars is significantly smaller than that of true Jupiter-mass planets. Based on this, we expect the incidence of brown dwarfs as false positives to be negligible, and we do not consider them here.

A white dwarf transiting a star can easily mimic the signal of a true Earth-size planet, since their sizes are comparable. Their masses, on the other hand, are of course very different. Some theoretical predictions suggest that binary stars consisting of a white dwarf and a main-sequence star may be as frequent as main-sequence binary stars (see, e.g., Farmer & Agol 2003). However, evidence so far from the *Kepler* mission seems to indicate that these predictions may be off by orders of magnitude. For example, none of the Earth-size candidates that have been monitored spectroscopically to determine their radial velocities (RVs) have shown any indication that the companion is as massive as a white dwarf. Also, while transiting white dwarfs with suitable periods would be expected to produce many easily detectable gravitational lensing events if their frequency were as high as predicted by Farmer & Agol (2003), no such magnification events compatible with lensing have been detected so far in the *Kepler* photometry (J. Jenkins 2012, private communication). For these reasons, we conclude that the relative number of eclipsing white dwarfs among the 196 Earth-size KOIs is negligible in comparison to other contributing sources of false positives.

3.6. Example of a False Positive Calculation

To illustrate the process of false positive estimation for planets of Earth size ($0.8 R_{\oplus} < R_p \leq 1.25 R_{\oplus}$), we present here the

calculation for a single case of a false positive involving a larger planet transiting a star physically bound to the *Kepler* target (Section 3.4), which happens to produce a signal corresponding to an Earth-size planet.

In this case selected at random, the target star (KIC 3453569) has a mass of $0.73 M_{\odot}$, a brightness of $Kp = 15.34$ in *Kepler* band, and a 3 hr CDPP of 133.1 ppm. As indicated above, the star has a 44% a priori chance of being a multiple system based on the work of Raghavan et al. (2010). We assign to the companion a mass and an orbital period drawn randomly from the corresponding distributions reported by these authors, with values of $0.54 M_{\odot}$ and 67.6 yr, corresponding to a semimajor axis of $a = 18.0$ AU.

This companion has an a priori chance F_{tp} of having a transiting planet equal to the number of KOIs (orbiting non-giant stars) divided by the number of non-giant stars ($F_{\text{tp}} = 2,302/132,756 = 0.017$) observed by *Kepler* in at least one quarter during the Q1–Q6 interval. We assign to this companion star a transiting planet drawn randomly from the Batalha et al. (2013) list of KOIs, with a radius of $1.81 R_{\oplus}$ (a super-Earth) and an orbital period of 13.7 days. The diluted depth of the signal of this transiting planet results in a 140 ppm dimming of the combined flux of the two stars during the transit, that could be incorrectly interpreted as an Earth-size planet ($0.91 R_{\oplus}$) transiting the target star. We set $T_{\text{depth}} = 1$, as this example pertains to false positives mimicking transits of Earth-size planets. Because of the smaller radius of the stellar companion ($R_{\text{comp}} = 0.707 R_{\odot}$, determined with the help of our representative 3 Gyr, solar-metallicity isochrone), that star has a correspondingly smaller chance that the planet we have assigned to orbit it will actually transit at the given period, compared to the median $\sim 1 R_{\odot}$ *Kepler* target. The corresponding correction factor is then $C_{\text{geom}} = 0.707$.

The correction C_{tpf} to the rate of occurrence of transiting planets acting as blends is the most complicated to estimate, as it relies in part on similar calculations carried out sequentially from the larger categories of planets, starting with the giant planets, as described earlier. For this example, we make use of the results of those calculations presented in Section 5. The C_{tpf} factor corrects the occurrence rate of planets in the $1.25\text{--}2 R_{\oplus}$ super-Earth category (since this is the relevant class for the particular blended planet we have simulated) for three distinct biases in the KOI list of Batalha et al. (2013), due to incompleteness, false positives, and the possible correlation of frequency with spectral type.

For our simulated planet with $R_p = 1.81 R_{\oplus}$ and $P = 13.7$ days, the incompleteness contribution to C_{tpf} was estimated by computing the S/N of the signals generated by a planet of this size transiting each individual *Kepler* target, using the CDPP of each target. We find that the transit signal could only be detected around 54.1% of the targets, from which the incompleteness boost is simply $1/0.541 = 1.848$. The contribution to C_{tpf} from the false positive bias was taken from Table 1 of Section 4 below, which summarizes the results from the bootstrap analysis mentioned earlier. That analysis indicates that the false positive rate for super-Earths is 8.8%, i.e., 91.2% of the KOIs in the $1.25\text{--}2 R_{\oplus}$ are transited by true planets. Finally, the third contributor to C_{tpf} addresses the possibility that small Neptunes from the KOI list acting as blends may be more common, for example, around stars of later spectral types than earlier spectral types. Our analysis in Section 6.4 in fact suggests that super-Earths have a uniform occurrence as a function of spectral type, and we account for this absence of correlation by setting

Table 1
False Positives for the Different Planet Size Classes

Class	Size Range	Involving Eclipsing Binaries		Involving Transiting Planets		Total	KOIs	FP Rate
		Background	Bound	Background	Bound			
Giants	6–22 R_{\oplus}	8.0 ± 3.1	4.7 ± 2.2	2.3 ± 1.7	24.5 ± 5.0	39.5 ± 6.4	223	$17.7\% \pm 2.9\%$
Large Neptunes	4–6 R_{\oplus}	5.5 ± 2.6	0.4 ± 0.4	1.4 ± 1.3	14.4 ± 3.8	21.7 ± 4.8	137	$15.9\% \pm 3.5\%$
Small Neptunes	2–4 R_{\oplus}	15.1 ± 4.3	0.2 ± 0.2	4.2 ± 2.2	46.6 ± 9.6	66.1 ± 10.7	985	$6.7\% \pm 1.1\%$
Super-Earths	1.25–2 R_{\oplus}	10.5 ± 3.6	0.05 ± 0.05	3.6 ± 2.1	44.1 ± 12.3	58.3 ± 13.0	666	$8.8\% \pm 1.9\%$
Earths	0.8–1.25 R_{\oplus}	5.5 ± 2.6	0.002 ± 0.002	2.2 ± 1.6	16.3 ± 5.0	24.1 ± 5.9	196	$12.3\% \pm 3.0\%$
Total		44.7 ± 7.3	5.3 ± 2.2	13.8 ± 4.1	146.0 ± 17.5	209.8 ± 19.6	2222	$9.4\% \pm 0.9\%$

Notes. The number of KOIs in the penultimate column corresponds to stars not considered here not to be giants ($\log g > 3.6$; Brown et al. 2011). Additionally, we have excluded the few KOIs outside of the radius range of interest here (0.8–22 R_{\oplus}).

a value of 1.0 for the spectral-type dependence correction factor. Combining the three factors just described, we arrive at a value of $C_{\text{tpf}} = 1.848 \times 0.912 \times 1.0 = 1.685$.

To ascertain whether this particular false positive could have been detected by *Kepler*, we compute its S/N as explained in the Appendix, in terms of the size of the small Neptune relative to the physically bound companion, the dilution factor from the target, the CDPP of the target, the number of transits observed (from the duration interval for the particular *Kepler* target divided by the period of the KOI), and the transit duration as reported by Batalha et al. (2013). The result, $S/N = 9.44$, is above the threshold (determined using the detection recovery rate studied in Section 5.1), so the signal would be detectable and we set $T_{\text{det}} = 1$.

With the above S/N, we may also estimate the angular size of the exclusion region outside of which the multi-quarter centroid motion analysis would rule out a blend. The value we obtain for the present example with the prescription given in the Appendix is $1''.1$. To establish whether the companion star is inside or outside of this region, we compute its angular separation from the target as follows. First, we estimate the distance to the system from the apparent magnitude of the target ($Kp = 15.34$) and the absolute magnitudes of the two stars, read off from our representative isochrone according to their masses of 0.73 and 0.54 M_{\odot} . Ignoring extinction, we obtain a distance of 730 pc. Next we place the companion at a random position in its orbit around the target, using the known semimajor axis of 18.0 AU and the random values of other relevant orbital elements (eccentricity, inclination angle, and longitude of periastron) as reported above. With this, the angular separation is $0''.02$. This is about a factor of 50 smaller than the limit from centroid motion analysis, so we conclude this false positive would not be detected in this way (i.e., it remains a viable blend). We therefore set $T_{\text{cent}} = 1$.

Finally, the formalism by Holman & Wiegert (1999) indicates that, to first order, a hierarchical triple system like the one in this example would be dynamically unstable if the companion star were within 1.06 AU of the target. As their actual mean separation is much larger ($a = 18.0$ AU), we consider the system to be stable and we set $T_{\text{stab}} = 1$.

Given the results above, this case is therefore a viable false positive that could be interpreted as a transiting Earth-size planet. The chance that this would happen for the particular *Kepler* target we have selected is given by the product $F_{\text{bin}} \times F_{\text{tp}} \times C_{\text{geom}} \times C_{\text{tpf}} \times T_{\text{depth}} \times T_{\text{det}} \times T_{\text{cent}} \times T_{\text{stab}} = 44\% \times 0.017 \times 0.707 \times (1.848 \times 0.912 \times 1.0) \times 1 \times 1 \times 1 \times 1 = 0.0089$. We performed similar simulations for each of the other *Kepler* targets observed between Q1 and Q6, and found that larger

planets transiting unseen companions to the targets are the dominant type of blend in this size class, and should account for a total of 16.3 false positives that might be confused with Earth-size planets. Doing the same for all other types of blends that might mimic Earth-size planets leads to an estimate of 24.1 false positives among the *Kepler* targets.

4. RESULTS FOR THE FALSE POSITIVE RATE OF *KEPLER*

The output of the simulations described above is summarized in Table 1, broken down by planet class and also by the type of scenario producing the false positive. We point out here again that these results are based on a revision of the detection model of *Kepler* (Section 5.1) rather than the a priori detection rate described in Section 3. An interesting general result is that the dominant source of false positives for all planet classes involves not eclipsing binaries, but instead large planets transiting an unseen companion to the *Kepler* target. This type of scenario is the most difficult to rule out in the vetting process performed by the *Kepler* team.

For giant planets, our simulations project a total of 39.5 false positives among the *Kepler* targets, or 17.7% of the 223 KOIs that were actually identified in this size category. This is significantly higher than the estimate from MJ11, who predicted a less than 5% false positive rate for this kind of objects. The relatively high frequency of false positives we obtain is explained by the inherently low occurrence of giant planets in comparison to the other astrophysical configurations that can mimic their signal. Another estimate of the false positive rate for giant planets was made recently by Santerne et al. (2012), from a sub-sample of KOIs they followed up spectroscopically. They reported that $34.8\% \pm 6.5\%$ of close-in giant planets with periods shorter than 25 days, transit depths greater than 0.4%, and brightness $Kp < 14.7$ show RV signals inconsistent with a planetary interpretation, and are thus false positives. Adopting the same sample restrictions, we obtain a false positive rate of $29.3\% \pm 3.1\%$, in good agreement with their observational result. This value is significantly larger than our overall figure of 17.7% for giant planets because of the cut at $P < 25$ days and the fact that the false positive rate increases somewhat toward shorter periods, according to our simulations (see Section 6.1).

For large Neptunes we find that the false positive rate decreases somewhat to 15.9%. This is due mainly to the lower incidence of blends from hierarchical triples, which can only mimic the transit depth of planets orbiting the largest stars in the sample, and to the relatively higher frequency of planets of this size in comparison to giant planets. The false positive rate

decreases further for small Neptunes and super-Earths, and rises again for Earth-size planets. The overall false positive rate of *Kepler* we find by combining all categories of planets is 9.4%.

All of these rates depend quite strongly on how well we have emulated the vetting process of *Kepler*. We may assess this as follows. We begin by noting that *before* the vetting process is applied, the majority of false positives are background eclipsing binaries. To estimate their numbers, we tallied all such systems falling within the photometric aperture of a *Kepler* target and contributing more than 50% of their flux (755 cases). Of these, 465 pass our secondary eclipse test (i.e., they present secondary eclipses that are detectable, and that have a depth differing by more than 3σ from the primary eclipse). After applying the centroid test we find that only 44.7 survive as viable blends. In other words, our simulated application of the centroid test rules out $465 - 44.7 \approx 420$ eclipsing binary blends. We may compare this with results from the actual vetting of *Kepler* as reported by Batalha et al. (2013), who indicated that 1093 targets from an initial list of 1390 passed the centroid test and were included as KOIs, and were added to the list of previously vetted KOIs from Borucki et al. (2011). The difference, $1390 - 1093 = 297$, is of the same order of magnitude as our simulated results (~ 420), providing a sanity check on our background eclipsing binary occurrence rates as well as our implementation of the vetting process. This exercise also shows that the centroid test is by far the most effective for weeding out blends. Even ignoring the test for secondary eclipses, the centroid analysis is able to bring down the number of blends involving background eclipsing binaries to only 83.3 out of the original 755 in our simulations, representing a reduction of almost 90%.

Due to the complex nature of the simulations it is non-trivial to assign uncertainties to the false positive rates reported in Table 1, and the values listed reflect our best knowledge of the various sources that may contribute. Many of the ingredients in our simulations rely on counts based directly on *Kepler* observations, such as the KOI list and the *Kepler* eclipsing binary catalog. For those quantities it is reasonable to adopt a Poissonian distribution for the statistical error (ϵ_{stat}). We have also attempted to include contributions from inputs that do not rely directly on *Kepler* observations. One is the uncertainty in the star counts that we have adopted from the Besançon model of Robin et al. (2003). A comparison of the simulated star densities near the center of the *Kepler* field with actual star counts (R. Gilliland 2010, private communication) shows agreement within 15%. We may therefore use this as an estimate of the error for false positives involving background stars (ϵ_{back}). As an additional test we compared the Besançon results with those from a different Galactic structure model. Using the Trilegal model of Girardi et al. (2005) we found that the stellar densities from the latter are approximately 10% smaller, while the distribution of stars in terms of brightness and spectral type is similar (background stars using Trilegal are only 0.47 mag brighter in the *R* band, and 100 K hotter, on average). We adopt the larger difference of 15% as our ϵ_{back} uncertainty.

We have also considered the additional uncertainty coming from our modeling of the detection level of the *Kepler* pipeline (ϵ_{detec}). While we initially adopted a nominal detection threshold corresponding to the expected detection rate following Jenkins et al. (2010a), in practice we find that this is somewhat optimistic, and below we describe a revision of that condition that provides better agreement with the actual performance of *Kepler* as represented by the published list of KOIs by Batalha et al. (2013). Experiments in which we repeated the

simulations with several prescriptions for the detection limit yielded a typical difference in the results compared to the model we finally adopted (see below) that may be used as an estimate of ϵ_{detec} . We note that the difference between the results obtained from all these detection prescriptions and those that use the a priori detection rate is approximately three times ϵ_{detec} . This suggests that the a priori detection model may be used to predict reasonable lower limits for the false positive rates, as well as the planet occurrence rates discussed later.

Based on the above, we take the total error for our false positive population involving background stars to be $\epsilon_{\text{tot}} = \sqrt{\epsilon_{\text{stat}}^2 + \epsilon_{\text{back}}^2 + \epsilon_{\text{detec}}^2}$. We adopt a similar expression for false positives involving stars physically associated with the target, without the ϵ_{back} term.

5. COMPUTING THE PLANET OCCURRENCE

The KOI list of Batalha et al. (2013) is composed of both true planets and false positives. The true planet population may be obtained by subtracting our simulated false positives from the KOIs. However, this difference corresponds only to planets in the *Kepler* field that both transit their host star and that are detectable by *Kepler*. In order to model the actual distribution of planets in each size class and as a function of their orbital period, we must correct for the geometric transit probabilities and for incompleteness. Our approach, therefore, is to not only simulate false positives, as described earlier, but to also simulate in detail the true planet population in such a way that the sum of the two matches the published catalog of KOIs, after accounting for the detectability of both planets and false positives. The planet occurrence rates we will derive correspond strictly to the average number of planets per star.

For our planet simulations we proceed as follows. We assign a random planet to each *Kepler* target that has been observed between Q1 and Q6, taking the planet occurrences per period bin and size class to be adjustable variables. We have elected to use the same logarithmic period bins as adopted by Howard et al. (2012) to ease comparisons, with additional bins for longer periods than they considered (up to ~ 400 days). We seek to determine the occurrence of planets in each of our five planet classes and for each of 11 period bins, which comes to 55 free parameters. We use the rates of occurrence found by Howard et al. (2012) for our initial guess (prior), with extrapolated values for the planet sizes (below $2 R_{\oplus}$) and periods (longer than 50 days) that they did not consider in their study. Each star is initially assigned a global chance of hosting a planet equal to the sum of these 55 occurrence rates. Our baseline assumption is that planet occurrence is independent of the spectral type of the host star, but we later investigate whether this hypothesis is consistent with the observations (i.e., with the actual distribution of KOI spectral types; Section 6).

We have also assumed that the planet sizes are logarithmically distributed between the size boundaries of each planet class, and that their periods are distributed logarithmically within each period bin. For each of our simulated planets we compute the geometric transit probability (which depends on the stellar radius) as well as the S/N of its combined transit signals (see the Appendix for details on the computation of the S/N). We assigned to each planet a random inclination angle, and discarded cases that are not transiting or that would not be detectable by *Kepler*. We assigned also a random eccentricity and longitude of periastron, with eccentricities drawn from a Rayleigh distribution, following Moorhead et al. (2011). These

authors found that such a distribution with a mean eccentricity in the range 0.1–0.25 provides a satisfactory representation of the distribution of transit durations for KOIs cooler than 5100 K. We chose to adopt an intermediate value for the mean of the Rayleigh distribution of $e = 0.175$, and used it for stars of all spectral types. Allowing for eccentric orbits alters the geometric probability of a transit as well as their duration (and thus their S/N). Finally, we compare our simulated population of detectable transiting planets with that of the KOIs minus our simulated false positives population, and we correct our initial assumption for the distribution of planets as a function of size and period.

To estimate uncertainties for our simulated true planet population we adopt a similar prescription as for the false positive rates, and compute $\epsilon_{\text{tot}} = \sqrt{\epsilon_{\text{stat}}^2 + \epsilon_{\text{detec}}^2}$, where the two contributions have the same meaning as before. While the two terms in ϵ_{tot} have roughly the same average impact on the global uncertainty, the statistical error tends to dominate when the number of KOIs in a specific size and period bin is small, and the detection error is more important for smaller planets and longer periods.

Modeling the detection limits of *Kepler* is a central component of the process, as the incompleteness corrections can be fairly large in some regimes (i.e., for small signals and/or long periods). Exactly how this is done affects both the false positive rates and the planet occurrence rates. We have therefore gone to some effort to investigate the accuracy of the nominal detection model (Section 3) according to which 50% of signals are considered detected by the *Kepler* pipeline if their S/N exceeds a threshold of 7.1, and 99.9% of signals are detected for an S/N over 10.1. We describe this in the following.

5.1. Detection Model

Burke et al. (2012) have reported that a significant fraction of the *Kepler* targets have not actually been searched for transit signals down to the official S/N threshold of 7.1. This is due to the fact that spurious detections with S/N over 7.1 can mask real planet signals with lower S/N in the same light curve. Pont et al. (2006) have shown that time-correlated noise features in photometric time series can produce spurious detections well over this threshold, and that this has significant implications for the yield of transit surveys. We note also that the vetting procedure that led to the published KOI list of Batalha et al. (2013) involves human intervention at various stages, and is likely to have missed some low-S/N candidates for a variety of reasons. Therefore, the assumption that most signals with S/N > 7.1 have been detected and are present in the KOI list is probably optimistic. Nevertheless, this hypothesis is useful in that it sets lower limits for the planet occurrence rates, and an upper limit for the false positive rates. For example, the overall false positive rate (all planet classes) we obtain when following the a priori detection rate is 14.9%, compared to our lower rate of 9.4% when using a more accurate model given below.

The clearest evidence that the *Kepler* team has missed a significant fraction of the low-S/N candidates is seen in Figure 1. This figure displays the distribution of the S/Ns of the actual KOIs, and compares it with the S/Ns for our simulated population of false positives and true planets. To provide for smoother distributions we have convolved the individual S/Ns with a Gaussian with a width corresponding to 20% of each S/N (a kernel density estimation technique). The S/Ns for the KOIs presented by Batalha et al. (2013) were originally computed

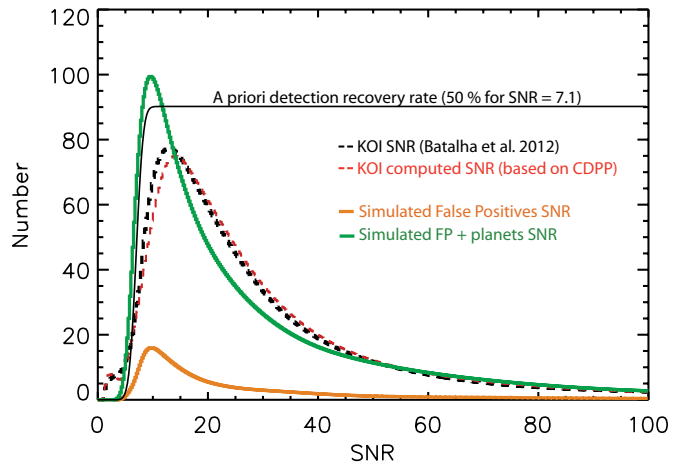


Figure 1. Comparison of signal-to-noise ratio distributions to evaluate the detection model (signal recovery rate) of *Kepler*. The dotted black curve corresponds to the KOIs from Batalha et al. (2013), with the S/Ns from their Table 9 adjusted to correspond to Q1–Q6, for consistency with our simulations (see the text). There is good agreement with the distribution of S/Ns computed from the CDPP (Christiansen et al. 2012; red curve). The green curve is the S/N distribution of our simulated population of false positives and true planets (which by construction matches the size/period distribution of actual KOIs). It assumes the nominal *Kepler* detection model in which 50% of the signals with S/N > 7.1 and 99.9% of the signals with S/N > 10.1 are detectable (solid black lines). The simulated false positives are shown separately by the orange curve. The dotted black curve peaks at a larger S/N than the green curve, indicating that the nominal detection model is not accurate: the effective recovery threshold must be significantly higher than 7.1.

(A color version of this figure is available in the online journal.)

based on observations from Q1 to Q8. For consistency with our simulations, which only use Q1–Q6, we have therefore degraded the published S/Ns accordingly. Also shown in the figure is the S/N distribution for the KOIs computed with the prescription described in the Appendix based on the CDPP (Christiansen et al. 2012). Several conclusions can be drawn. One is that there is very good agreement between the S/Ns computed by us from the CDPP (red line) and those presented by Batalha et al. (2013; adjusted to Q1–Q6; black line). Importantly, this validates the CDPP-based procedure used in this paper to determine the detectability of a signal. It also suggests that the KOI distribution contains useful information on the actual signal recovery rate of *Kepler*. Second, we note that a small number of KOIs (~70) have S/Ns (either computed from the CDPP or adjusted to Q1–Q6) that are actually below the nominal threshold of 7.1. Most of these lower S/Ns are values we degraded from Q1–Q8 to Q1–Q6, and others are for KOIs that were not originally found by the *Kepler* pipeline, but were instead identified later by further examination of systems already containing one or more candidates. Third and most importantly, the peak of the S/N distribution from our simulations (green line in the figure), which by construction match the size and period distributions of the KOIs and use the a priori detection model, is shifted to smaller values than the one for KOIs. This suggests that the a priori detection model described in Section 3 in which 50% of the signals with S/N > 7.1 (and 99.9% of the signals S/N > 10.1) have been detected as KOIs is not quite accurate, and indicates the detection model requires modification.

It is not possible to adjust the S/N-dependent recovery rate simultaneously with the occurrence rates of planets in our simulations, as the two are highly degenerate. However, we find that we are able to reach convergence if we assume the following.

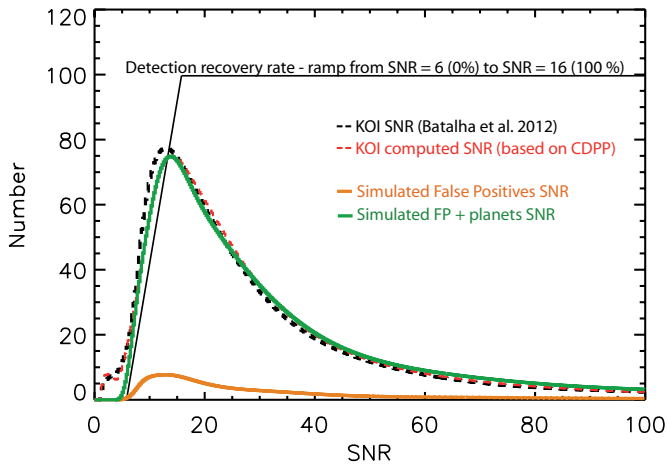


Figure 2. Same as Figure 1 but with a detection model (solid black lines) ranging linearly from 0% for candidates with an S/N of 6 or lower to 100% for candidates above an S/N of 16. With this model our simulations can match not only the size and period distribution of KOIs, but also the distribution of their S/Ns.

(A color version of this figure is available in the online journal.)

1. The recovery rate is represented by a monotonically rising function, rather than a fixed threshold, increasing from zero at some low S/N to 100% for some higher S/N.
2. The model for the recovery rate function should allow for a good match of the distribution of S/Ns separately for each of our five planet classes.

A number of simple models were tried, and we used the Bayesian Information Criterion (BIC) to compare them and make a choice: $\text{BIC} = \chi^2 + k \ln n$. In this expression, χ^2 was computed in the usual way by comparing our simulated S/Ns for the population of false positives and true planets with the one for the KOIs; k is the number of free parameters of the model, and n is the number of bins in the histogram of the S/N distributions. We considered the five planet categories at the same time and computed the BIC by summing up the corresponding χ^2 values, with n therefore being the sum of the number of bins for all classes. The model that provides the best BIC involves a simple linear ramp for the recovery rate between S/Ns of 6 and 16; in other words, no transit signal with an S/N below 6 is recovered, and every transit signal is recovered over 16. Figure 2 (to be compared with Figure 1) shows the much better agreement between the S/N distribution of our simulated population of false positives and planets, and the S/Ns for the KOIs. We adopt this detection model for the remainder of the paper.

6. PLANET OCCURRENCE RESULTS

This section presents the results of our joint simulation of false positives and true planets for each of the planet categories, and compares their distributions with those of actual KOIs from Batalha et al. (2013). In particular, since we have assumed no correlation between the planet frequencies and the spectral type of the host star (the simplest model), here we examine whether there is any such dependence, using the stellar mass as a proxy for spectral type. As in some of the previous figures, we display generalized histograms computed with a kernel density estimator approach in which the stellar masses are convolved with a Gaussian function. We adopt a Gaussian width (σ) of 20%, which we consider to be a realistic estimate of the mass uncertainties in the KIC.

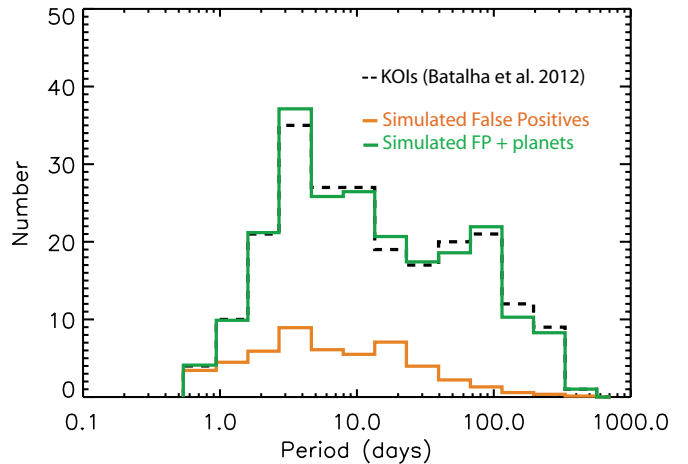


Figure 3. Histogram of the periods of giant planet KOIs from Batalha et al. (2013) (dotted black lines), simulated false positives (orange), and the sum of simulated false positives and simulated planets (green).

(A color version of this figure is available in the online journal.)

The total frequencies (average number of planets per star) are reported in Tables 2 and 3. The first table presents the occurrence of planets of different classes per period bin of equal size on a logarithmic scale. The bin with the longest period for which we can provide an occurrence estimate differs for the different planet classes. We do not state results for period bins in which the number of KOIs is less than 1σ larger than the number of false positives; for these size/period ranges the current list of *Kepler* candidates is not large enough to provide reliable values. Cumulative rates of occurrence of planets as a function of period are presented in Table 3. Another interesting way to present planet occurrence results is to provide the number of stars that have at least one planet in various period ranges. This requires a different treatment of KOIs with multiple planet candidates for the same star. To compute these numbers, shown in Table 4, we repeated our simulations by removing from the KOI list the planet candidates beyond the inner one in the considered size range, for KOIs with multiple candidates.

6.1. Giant Planets ($6-22 R_{\oplus}$)

Planet occurrence rates and false positive rates are interdependent. As described earlier, the bootstrap approach we have adopted to determine those properties for the different planet classes begins with the giant planets, as only larger objects (stars) with well understood properties can mimic their signals. The process then continues with smaller planets in a sequential fashion.

The frequencies of giant planets per period bin were adjusted until their distribution added to that of false positives reproduces the period spectrum of actual KOIs. This is illustrated in Figure 3, where the simulated and actual period distributions (green and dotted black lines) match on average, though not in detail because of the statistical nature of the simulations. The frequency of false positives (orange line) is seen to increase somewhat toward shorter periods, peaking at $P \sim 3-4$ days. Similar adjustments to the frequencies by period bin have been performed successively for large Neptunes, small Neptunes, super-Earths, and Earth-size planets.

We find that the overall frequency of giant planets (planets per star) in orbits with periods up to 418 days is close to 5.2%. Figure 4 (top panel) displays the distribution of simulated false positives for this class of planets as a function of the mass of

Table 2
Average Number of Planets Per Star Per Period Bin (in Percent)

Class	Period Range (days)										
	0.8– 2.0	2.0– 3.4	3.4– 5.9	5.9– 10	10– 17	17– 29	29– 50	50– 85	85– 145	145– 245	245– 418 ^a
Giants	0.015	0.067	0.17	0.18	0.27	0.23	0.35	0.71	1.25	0.94	1.05
	±0.007	±0.018	±0.03	±0.04	±0.06	±0.06	±0.10	±0.17	±0.29	±0.28	±0.30
Large Neptunes	0.004	0.006	0.11	0.091	0.29	0.32	0.49	0.66	0.43	0.53	0.24
	±0.003	±0.006	±0.03	±0.030	±0.07	±0.08	±0.12	±0.16	±0.17	±0.21	±0.15
Small Neptunes	0.035	0.18	0.73	1.93	3.67	5.29	6.45	5.25	4.31	3.09	...
	±0.011	±0.03	±0.09	±0.19	±0.39	±0.64	±1.01	±1.05	±1.03	±0.90	...
Super-Earths	0.17	0.74	1.49	2.90	4.30	4.49	5.29	3.66	6.54
	±0.03	±0.13	±0.23	±0.56	±0.73	±1.00	±1.48	±1.21	±2.20
Earths	0.18	0.61	1.72	2.70	2.70	2.93	4.08	3.46
	±0.04	±0.15	±0.43	±0.60	±0.83	±1.05	±1.88	±2.81
Total	0.41	1.60	4.22	7.79	11.2	13.3	16.7	13.7
	±0.05	±0.20	±0.50	±0.85	±1.2	±1.6	±2.6	±3.2

Notes. Planet occurrence per period bin for each class of planet defined in Section 2.2. The first line in each group represents planet occurrences (in percent), and the second line gives their error bars. The increase in the uncertainties relative to the occurrence rates toward longer periods is due to the drop in the geometric transit probability and detection rate. Empty fields for the smallest planets occur where the *Kepler* results based on six quarters of data are insufficient to provide an estimate.

^a For planets with long periods, we have assumed that two transits are sufficient for a detection. We have also corrected the planet occurrences for periods longer than half the total duration of the Q1–Q6 survey (670 days), to account for the fact that a fraction of these long period planets would have shown a single transit in the Q1–Q6 survey, depending on the transit date.

Table 3
Average Number of Planets Per Star for Different Period Ranges (in Percent)

Class	Period Range (days)										
	0.8– 2.0	0.8– 3.4	0.8– 5.9	0.8– 10	0.8– 17	0.8– 29	0.8– 50	0.8– 85	0.8– 145	0.8– 245	0.8– 418
Giants	0.015	0.082	0.25	0.43	0.70	0.93	1.29	2.00	3.24	4.19	5.24
	±0.007	±0.019	±0.04	±0.05	±0.08	±0.10	±0.14	±0.22	±0.37	±0.46	±0.55
Large Neptunes	0.004	0.010	0.12	0.21	0.50	0.82	1.31	1.97	2.41	2.94	3.18
	±0.003	±0.007	±0.03	±0.04	±0.08	±0.11	±0.17	±0.23	±0.29	±0.36	±0.39
Small Neptunes	0.035	0.22	0.95	2.88	6.55	11.8	18.3	23.5	27.8	30.9	...
	±0.011	±0.03	±0.10	±0.21	±0.44	±0.8	±1.3	±1.6	±1.9	±2.1	...
Super-Earths	0.17	0.91	2.40	5.30	9.60	14.1	19.4	23.0	29.6
	±0.03	±0.13	±0.27	±0.62	±0.96	±1.4	±2.0	±2.4	±3.2
Earths	0.18	0.79	2.51	5.21	7.91	10.8	14.9	18.4
	±0.04	±0.16	±0.46	±0.76	±1.13	±1.5	±2.4	±3.7
Total	0.41	2.0	6.2	14.0	25.3	38.5	55.2	68.9
	±0.05	±0.2	±0.5	±1.0	±1.6	±2.2	±3.4	±4.7

Notes. Cumulative planet occurrence rates in each period bin for the planet classes defined in Section 3. The top line for each group is the cumulative occurrence rate (in percent), and the bottom line corresponds to the uncertainty.

Table 4
Percentage of Stars with at Least One Planet for Different Period Ranges

Class	Period Range (days)										
	0.8– 2.0	0.8– 3.4	0.8– 5.9	0.8– 10	0.8– 17	0.8– 29	0.8– 50	0.8– 85	0.8– 145	0.8– 245	0.8– 418
Giants	0.015	0.082	0.25	0.43	0.70	0.93	1.29	1.97	3.19	4.09	5.12
	±0.007	±0.019	±0.04	±0.05	±0.08	±0.10	±0.14	±0.22	±0.36	±0.46	±0.55
Large Neptunes	0.004	0.010	0.12	0.21	0.49	0.80	1.23	1.86	2.26	2.76	2.99
	±0.003	±0.007	±0.03	±0.04	±0.08	±0.11	±0.17	±0.24	±0.29	±0.36	±0.39
Small Neptunes	0.031	0.20	0.89	2.61	5.82	10.24	15.48	19.90	23.41	26.00	...
	±0.011	±0.04	±0.09	±0.18	±0.34	±0.54	±0.84	±1.19	±1.44	±1.65	...
Super-Earths	0.16	0.83	2.20	4.82	8.63	12.54	17.09	20.31	26.11
	±0.03	±0.12	±0.23	±0.53	±0.79	±1.12	±1.61	±1.95	±2.87
Earths	0.18	0.75	2.39	4.86	7.30	9.83	13.49	16.55
	±0.09	±0.17	±0.44	±0.69	±1.04	±1.40	±2.27	±3.60
Any Planet	0.35	1.43	4.58	9.87	19.24	29.57	40.45	52.26
	±0.05	±0.15	±0.39	±0.70	±1.21	±1.78	±2.73	±4.16

Note. The top line in each group represents the number of stars that have at least one planet in that period range (in percent), and the bottom line corresponds to the uncertainty.

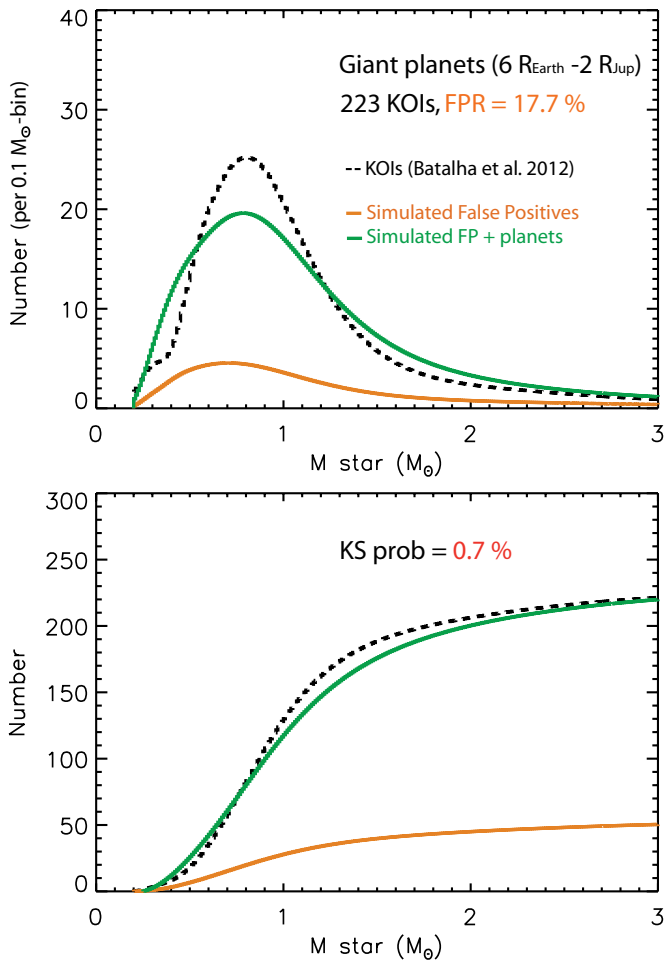


Figure 4. Top: generalized histogram of the stellar masses of KOI host stars in the giant planet category (dotted black curve), compared against the results of our Monte Carlo simulation of the *Kepler* targets observed during Q1–Q6. The total number of KOIs with main-sequence host stars in this category (223) and the overall false positive rate (FPR = 17.7%; Table 1) are indicated. Simulated false positives are shown in orange, and the sum of these and the simulated planet population are represented in green. The green and dotted black curves are statistically different. Bottom: cumulative distribution of stellar masses from the top panel. Our assumed uniform occurrence of giant planets as a function of the host star spectral type (mass) results in a distribution that is statistically different from the actual KOI distribution (K-S probability of 0.7%). The KOI distribution indicates that G–K stars are more likely to host giant planets than F- and M-type stars.

(A color version of this figure is available in the online journal.)

the host star (orange curve). After adding to these the simulated planets, we obtain the green curve that represents stars that either have a true transiting giant planet or that constitute a false positive mimicking a planet in this category. The comparison with the actual distribution of KOIs (black dotted curve) shows significant differences, with a Kolmogorov–Smirnov (K-S) probability of 0.7%. This suggests a possible correlation between the occurrence of giant planets and spectral type (mass), whereas our simulations have assumed none. In particular, the simulations produce an excess of giant planets around late-type stars, implying that in reality there may be a deficit for M dwarfs. The opposite seems to be true for G and K stars. Doppler surveys have also shown a dependence of the rates of occurrence of giant planets with spectral type. For example, Johnson et al. (2010) reported a roughly linear increase as a function of stellar mass, with an estimate of about 3% for M dwarfs. We find a similar figure of $3.6\% \pm 1.7\%$. As is the case for the RV surveys, our

frequency increases for G and K stars to $6.1\% \pm 0.9\%$, but then reverses for F (and warmer) stars to $4.3\% \pm 1.0\%$, while the Doppler results suggest a higher frequency approaching 10%. We point out, however, that there are rather important differences between the two samples: (1) the estimates from RV surveys extend out to orbital separations of 2.5 AU, while our study is only reasonably complete to periods of ~ 400 days (1.06 AU for a solar-type star); (2) the samples are based on two very different characteristics: the planet mass for RV surveys, and planet radius for *Kepler*; and (3) there may well be a significant correlation between the period distribution of planets and their host star spectral type. Indeed, the results from the study of planets orbiting A-type stars by Bowler et al. (2010) provides an explanation for the apparent discrepancy between RV and *Kepler* results for the occurrence of giant planets orbiting hot stars: Figure 1 of the above paper shows that no Doppler planets have been discovered with semimajor axes under 0.6 AU for stellar masses over $1.5 M_{\odot}$, creating a “planet desert” in that region. Thus, the Doppler surveys find the more common longer-period planets around the hotter stars, and *Kepler* has found the rarer planets close-in.

Averaged over all spectral types, the frequency of giant planets up to orbital periods of 418 days is approximately 5.2% (Table 3).

6.2. Large Neptunes ($4\text{--}6 R_{\oplus}$)

Our simulations result in an overall frequency of large Neptunes with periods up to 418 days of approximately 3.2%. The distribution in terms of host star mass is shown in Figure 5, and indicates a good match to the distribution of the large Neptune-size KOIs from Batalha et al. (2013; K-S probability of 23.3%). We conclude that there is no significant dependence of the occurrence rate of planets in this class with the spectral type of the host star.

6.3. Small Neptunes ($2\text{--}4 R_{\oplus}$)

The overall rate of occurrence (planets per star) of small Neptunes rises significantly compared to that of larger planets, reaching 31% out to periods of 245 days. Due to small number statistics, we are unable to provide reliable estimates for periods as long as those considered for the larger planets (up to 418 days). The logarithmic distribution of sizes we have assumed within each planet category allows for a satisfactory fit to the actual KOI distributions in each class (with separate K-S probabilities above 5%), with the exception of the small Neptunes. As noted earlier, the increase in planet occurrence toward smaller radii for these objects is very steep (Figure 7). We find that dividing the small Neptunes into two subclasses (two radius bins of the same logarithmic size: $2\text{--}2.8 R_{\oplus}$ and $2.8\text{--}4 R_{\oplus}$) we are able to obtain a much closer match to the KOI population (K-S probability of 6%) with similar logarithmic distributions within each sub-bin as assumed before.

In our analysis, we have deliberately chosen the size range for small Neptunes to be the same as that adopted by Howard et al. (2012), to facilitate the comparison with an interesting result they reported in a study based on the first three quarters of *Kepler* data. They found that small Neptunes are more common around late-type stars than early-type stars, and that the chance, $f(T_{\text{eff}})$, that a star has a planet in the $2\text{--}4 R_{\oplus}$ range depends roughly linearly on its temperature. Specifically, they proposed $f(T_{\text{eff}}) = f_0 + k_T(T_{\text{eff}} - 5100 \text{ K})/1000 \text{ K}$, valid over the temperature range from 3600 K to 7100 K, with coefficients $f_0 = 0.165 \pm 0.011$ and $k_T = -0.081 \pm 0.011$.

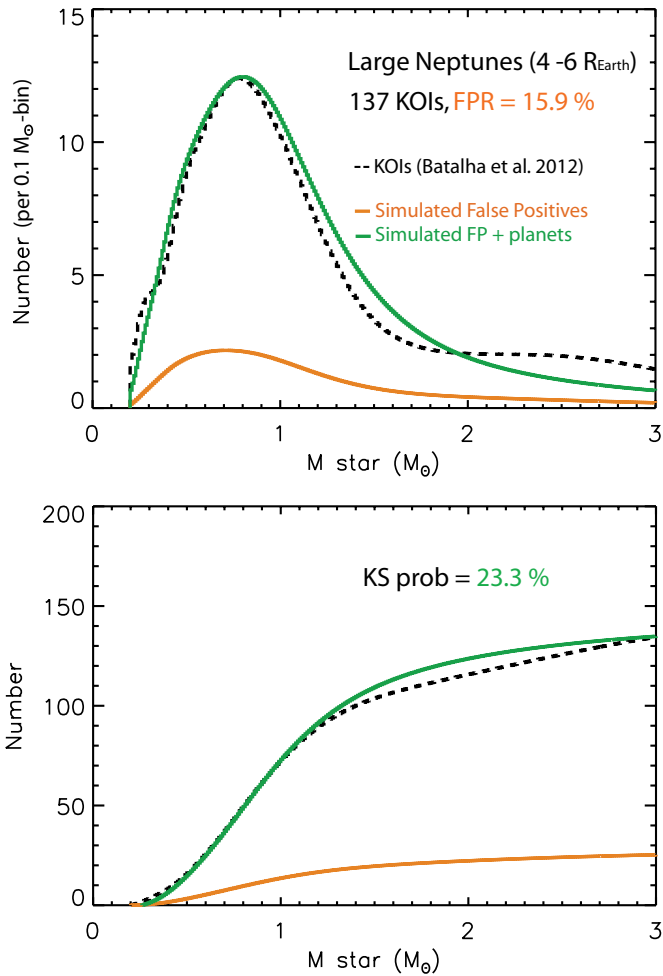


Figure 5. Similar to Figure 4, for the large Neptunes. In this case, the mass distributions of KOIs and simulated false positives and planets are statistically indistinguishable (K-S probability = 23.3%), supporting the lack of any correlation of the planet frequency with spectral type for this class of objects. (A color version of this figure is available in the online journal.)

In addition to the use in the present work of the considerably expanded KOI list from Batalha et al. (2013) (which is roughly twice the size of the KOI list from Borucki et al. 2011 used by Howard et al. 2012), there are a number of other significant differences between our analysis and theirs including the fact that we account for false positives, and we use a different model for the detection efficiency of *Kepler*. It is of considerable interest, therefore, to see if their result still holds, as it could provide important insights into the process of planet formation and/or migration.

We first repeated our analysis as before, with no assumed dependence of the planet frequencies on the spectral type of the host star, but we adjusted other assumptions to match those of Howard et al. (2012). Instead of our modified detection model (linear ramp; Section 5.1), we adopted a fixed S/N threshold of 10, as they did. Also, rather than assuming logarithmic distributions within each of our sub-bins (which Howard et al. 2012 also considered), we assigned to each planet a radius equal to the value corresponding to the center of the bin from Howard et al. (2012), as they did. Adopting the same linear relation $f(T_{\text{eff}})$ proposed by Howard et al. (2012), a least-squares fit to the frequencies from our simulations as a function of host star effective temperature yielded the coefficients $f_0 = 0.170$ and $k_T = -0.082$, in very good agreement with their results.

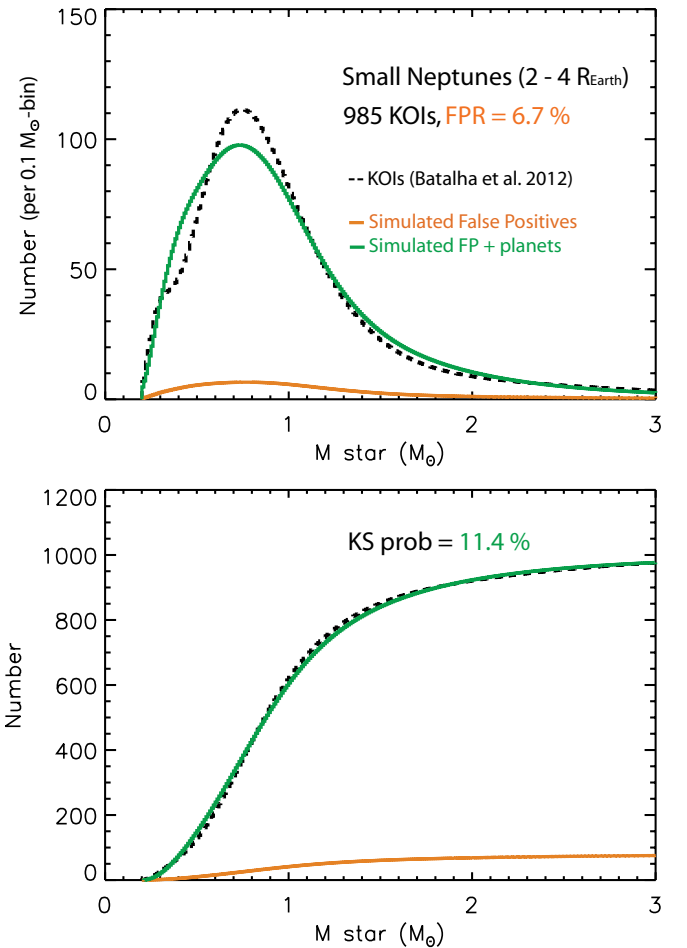


Figure 6. Similar to Figure 4, for the small Neptunes. A K-S test indicates there is no significant correlation between planet occurrence and stellar mass. (A color version of this figure is available in the online journal.)

However, returning to the assumptions of our work in this paper (linear ramp detection model, logarithmic/quadratic size distribution, and false positive corrections), we find that the correlation between planet occurrence and spectral type (or equivalently T_{eff} , or mass) for the small Neptunes all but disappears (Figure 6): a K-S test indicates that the KOI distribution and our simulated population of false positives and true planets (with the assumption of no mass dependence) are not significantly different (false alarm probability = 11.4%). Thus, we do not confirm the Howard et al. (2012) finding.

A number of results from our simulations help to explain why we see no dependence of the planet frequency on spectral type, whereas Howard et al. (2012) did. One is that the median S/N for small Neptunes (detectable or not) in our simulated sample is 12.5, a value for which we have shown that the KOI list is likely incomplete (see Section 5.1). This means that a significant number of small Neptunes in the *Kepler* field have not been recovered as KOIs, especially those transiting larger stars. Second, we find that the distribution of sizes inside the small Neptune class rises sharply toward smaller radii. This is shown in Figure 7. Since these more numerous smaller planets are easier to detect around late-type stars, this artificially boosts the occurrence of planets around such stars. Third, the false positive rate is slightly higher for later-type stars, again resulting in a higher planet occurrence around those stars, if not corrected for.

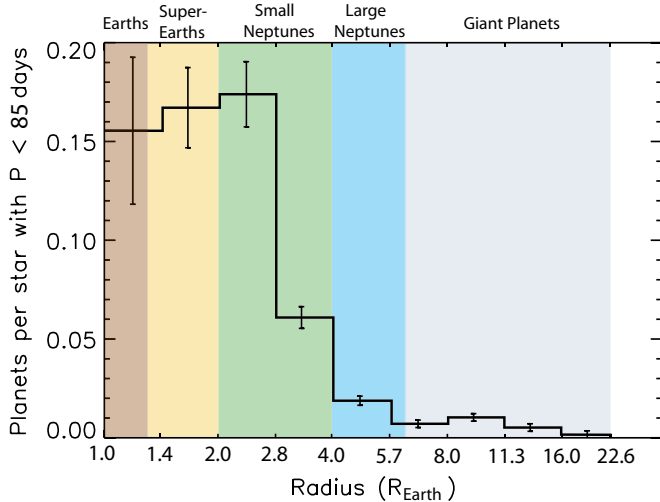


Figure 7. Average number of planets per size bin for main-sequence FGKM stars, determined here from the Q1–Q6 *Kepler* data and corrected for false positives and incompleteness.

(A color version of this figure is available in the online journal.)

6.4. Super-Earths ($1.25\text{--}2 R_{\oplus}$)

According to our simulations the overall average number of super-Earths per star out to periods of 145 days is close to 30%. The distribution of host star masses for the super-Earths is shown in Figure 8. While there is a hint that planets of this size may be less common around M dwarfs than around hotter stars, a K-S test indicates that the simulated and real distributions are not significantly different (false alarm probability of 4.9%).

6.5. Earths ($0.8\text{--}1.25 R_{\oplus}$)

As indicated in Table 3, the overall rate of occurrence (average number of planets per star) we find for Earth-size planets is 18.4%, for orbital periods up to 85 days. Similarly to the case for larger planets, our simulated population of false positives and Earth-size planets is a good match to the KOIs in this class, without the need to invoke any dependence on the mass of the host star (see Figure 9).

Among the Earth-size planets that we have randomly assigned to KIC target stars in our simulations, we find that approximately 23% have S/Ns above 7.1, but only about 10% would be actually detected according to our ramp model for the *Kepler* recovery rate. These are perhaps the most interesting objects from a scientific point of view. Our results also indicate that 12.3% of the Earth-size KOIs are false positives (Table 1). This fraction is small enough to allow statistical analyses based on the KOI sample, but is too large to claim that any individual Earth-size KOI is a bona fide planet without further examination. Ruling out the possibility of a false positive is of critical importance for the goal of confidently detecting the first Earth-size planets in the habitable zone of their parent star.

On the basis of our simulations we may predict the kinds of false positives that can most easily mimic an Earth-size transit, so that observational follow-up efforts may be better focused toward the validation of the planetary nature of such a signal. Figure 10 shows a histogram of the different kinds of false positives that result in photometric signals similar to Earth-size transiting planets, as a function of their magnitude difference compared to the *Kepler* target.

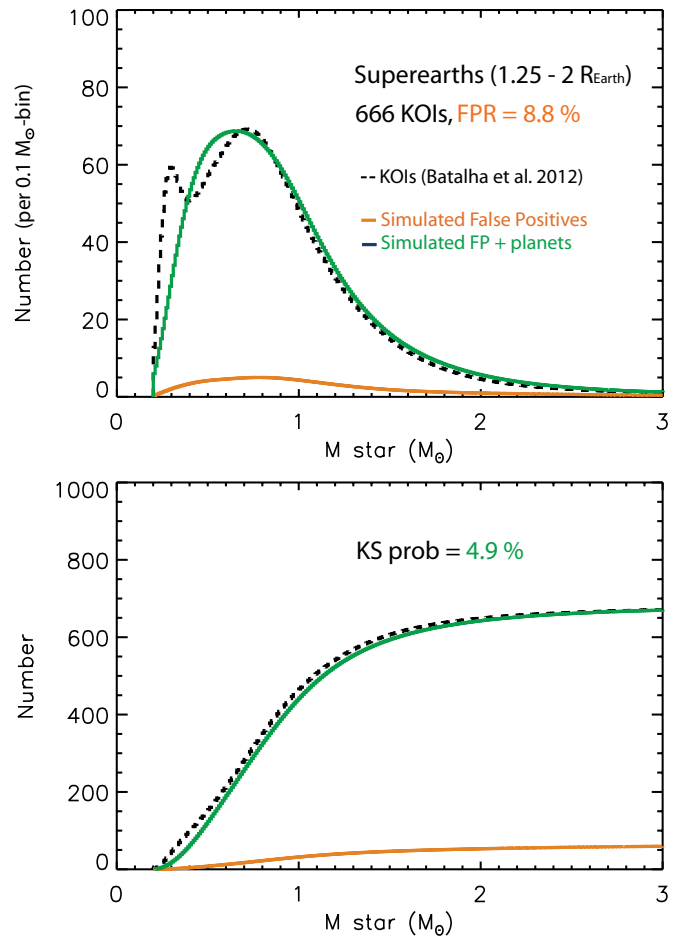


Figure 8. Similar to Figure 4, for super-Earths.

(A color version of this figure is available in the online journal.)

There are two dominant sources of false positives for this class of signals. One is background eclipsing binaries, most of which are expected to be between 8 and 10 mag fainter than the *Kepler* target in the *Kp* passband, and some will be even fainter. The most effective way of ruling out background eclipsing binaries is by placing tight limits on the presence of such contaminants as a function of angular separation from the target. In previous planet validations with BLENDER (e.g., Fressin et al. 2011, 2012b; Cochran et al. 2011; Borucki et al. 2012) the constraints from ground-based high spatial resolution adaptive optics imaging have played a crucial role in excluding many background stars beyond a fraction of an arcsecond from the target. However, these observations typically only reach magnitude differences up to 8–9 mag (e.g., Batalha et al. 2011), and such dim sources can only be detected at considerably larger angular separations of several arcsecond. Any closer companions of this brightness would be missed. Since background eclipsing binaries mimicking an Earth-size transit can be fainter still, other more powerful space-based resources may be needed in some cases such as coronagraphy or imaging with the *Hubble Space Telescope*.

Another major contributor to false positives, according to Figure 10, is larger planets transiting a physically bound companion star. In this case, the angular separations from the target are significantly smaller than for background binaries, and imaging is of relatively little help. Nevertheless, considerable power to rule out such blends can be gained from high-S/N

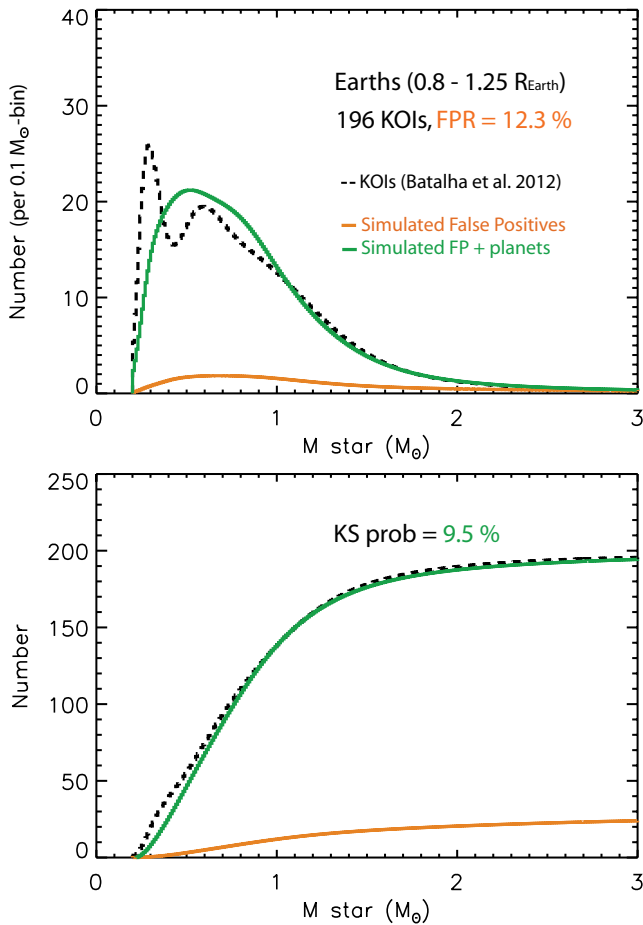


Figure 9. Similar to Figure 4, for Earth-size planets.

(A color version of this figure is available in the online journal.)

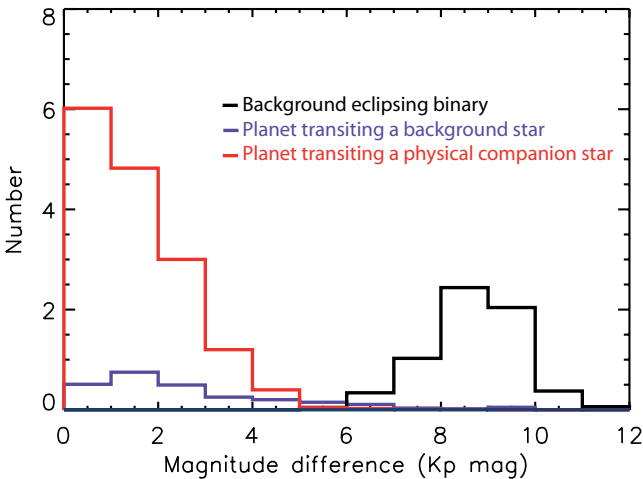


Figure 10. Histogram of the magnitude difference (in the *Kepler* band) relative to the target of the various kinds of false positives that could be interpreted as a transiting Earth-size planet. Background eclipsing binaries and larger planets transiting a physically associated star are the main sources, with larger planets transiting background stars being less important. Eclipsing binaries bound to the target produce signals that are typically too deep to be confused with an Earth.

(A color version of this figure is available in the online journal.)

spectroscopic observations in the optical or near-infrared, which can provide useful limits on the presence of very close companions in the form of maximum companion brightness as a function of RV difference compared to the target.

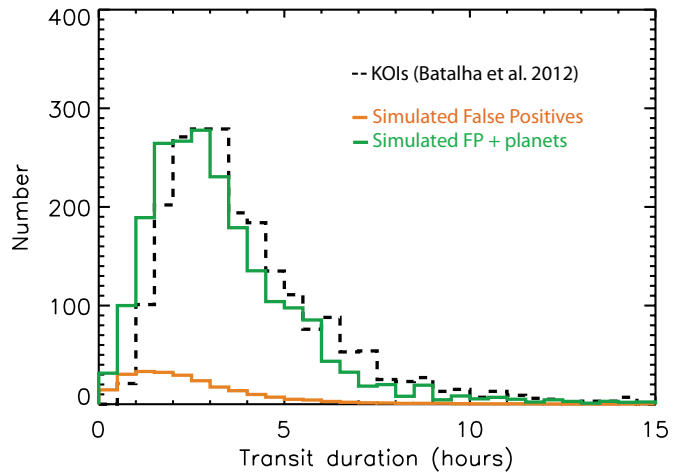


Figure 11. Histogram of the transit durations for the total population of KOIs from Earth-size to giant planets (dotted black line), simulated false positives (orange), and the sum of the simulated false positives and simulated planets (green). The excess of simulated false positives and planets with very short durations, in comparison with the KOI distribution, is mainly due to the fact that the *Kepler* pipeline was not designed to extract candidates with durations less than 1 hr.

(A color version of this figure is available in the online journal.)

7. TRANSIT DURATIONS

An additional result of interest from the present study concerns the transit durations. Figure 11 shows the distribution of durations for our simulated false positives and planets (all sizes) compared with the distribution for the KOIs from Batalha et al. (2013). We find an excess of short durations, some under 1 hr. This is likely explained by the fact that the *Kepler* pipeline is only designed, in principle, to search for transits with durations between 1 and 16 hr (Jenkins et al. 2010a). These short-duration transits have been included in our simulations because even though they were nominally not searched for, some KOIs in the list of Batalha et al. (2013) actually do have such short durations. More importantly, this result suggests that there should actually be more than 100 additional planets with such extremely short durations that may be detectable in the light curves. Efforts to look for them may reveal an interesting and unexplored population.

8. DISCUSSION

We have endeavored in this work to adopt assumptions that are as reasonable and realistic as is practical, in order to ensure the results are as accurate as possible. We have gone to considerable lengths to test and adopt a sensible model for the detection efficiency of *Kepler*, we have used informed estimates of quantities such as number densities of stars, frequencies of binaries and multiple systems, and frequencies of eclipsing binaries in the *Kepler* field, and we have taken into account numerous other details in our simulations that similar studies have generally not considered. These efforts notwithstanding, unavoidable idiosyncrasies in the way the *Kepler* photometry is handled and in the process by which the most recent catalog of KOIs was assembled mean that it is very difficult to avoid subtle biases when extracting information on the false positive rate and the frequencies of planets from this somewhat inhomogeneous data set.

One example of these difficulties is the vetting process followed by the *Kepler* team. It is quite likely that this procedure

has rejected more false positives than we have in our simulations, especially for the high-S/N candidates, because of the application of additional criteria based on the light curves themselves. For instance, information on the shape of the transits, which is not explicitly used in our work, can be extremely useful for excluding blends, as demonstrated forcefully in a number of validation studies of *Kepler* candidates with BLENDER (e.g., Cochran et al. 2011; Ballard et al. 2011; Fressin et al. 2012a; Gautier et al. 2012; Borucki et al. 2012). This can often reduce the false positive frequencies by orders of magnitude. It is reasonable to assume that interesting photometric signals have only been promoted to KOIs by the *Kepler* team if an acceptable fit to the light curve was possible with a transit model. However, estimating how many signals were rejected because of a poor fit is non-trivial, and is further complicated when the shapes are distorted (widened) by unrecognized transit timing variations. In any case, this would mostly involve cases with relatively high S/N where the shape is well defined, such as larger planets with multiple transits. Therefore, this criterion would generally only rule out false positives involving larger eclipsing objects, and not blends involving other planets or very small stars, which constitute the majority of false positive sources.

On the other hand, not all KOIs in the catalog of Batalha et al. (2013) have been subjected to the same level of vetting. For example, the KOIs from the earlier list by Borucki et al. (2011), which were incorporated into the new catalog, did not benefit from a systematic multi-quarter centroid motion analysis as newer candidates did, and may therefore have a somewhat higher rate of false positives.

This effect and the one described previously will tend to compensate each other, and as a result we do not believe the false positive rates in Table 1 should be much affected, particularly since the biases would mostly influence scenarios involving eclipsing binaries rather than stars transited by larger planets, and the former happen to be less numerous.

An additional source of error in our analysis comes from possible biases in the stellar characteristics provided in the KIC, reported by a number of authors. Pinsonneault et al. (2012) found effective temperatures that are typically ~ 200 K hotter than listed in the KIC. Muirhead et al. (2012) reported that the masses and radii for cool stars with $T_{\text{eff}} < 4400$ K are overestimated, a result confirmed by Dressing & Charbonneau (2013). The latter authors also found support for the earlier result by Mann et al. (2012) that nearly all (93%–97%) of the bright and cool unclassified stars in the KIC with $Kp < 14$ and $T_{\text{eff}} < 4000$ K are giants. The systematic errors in the KIC stellar parameters are likely to affect the estimated planetary radii (blurring or shifting the boundaries of the different planet classes), and may also impact our results regarding the correlation (or lack thereof) between the occurrence of small planets (small Neptunes and super-Earths) and spectral type, to some extent, possibly changing the global false positive rate and planet occurrence results.

There are also some indications of possible biases in the fitted transit parameters reported by Batalha et al. (2013). For example, the median impact parameter of the entire sample is 0.706, which seems inconsistent with an isotropic distribution of inclination angles. The impact parameter is typically correlated with the normalized semimajor axis a/R_* in the fits (related to the duration), as well as with the transit depth ($\propto R_p^2/R_*^2$). There is the potential, therefore, for additional systematic errors in the estimated radii for the planet candidates, and in the durations, which may explain part of the differences noted in Figure 11.

Another factor that can influence the durations is the orbital eccentricity distribution. The overall effect of increasing the eccentricities for the simulated planets is to shift the duration distribution slightly toward smaller values. This can be understood by realizing that, although transits occurring near apastron last longer, the chance that they will happen is smaller than transits occurring when the planet is closer to the star. This connection between eccentricities and transit durations may in fact be exploited to characterize the distribution of planetary eccentricities using the durations, as done by Moorhead et al. (2011) based on an earlier release of candidates from the first two quarters of *Kepler* observations (Borucki et al. 2011). We have refrained from pursuing such a project here with the updated candidate list, as we believe uncertainties in the stellar parameters from the KIC, the transit parameters, and in the efficiency of the *Kepler* detection pipeline for very short durations are still too important to allow an unbiased characterization of the eccentricity distribution.

9. CONCLUSIONS

The *Kepler* mission was conceived with the objective of determining the frequency of Earth-size and larger planets, including the ones in or near the habitable zone of their parent stars, and determining their properties. This eminently statistical goal requires a good understanding of the false positive rate among planet candidates, and of the actual detection capability of *Kepler*.

In this work we have developed a detailed simulation of the entire *Kepler* transit survey based on observations from quarters 1 through 6, designed to extract information on the occurrence rates of planets of different sizes as a function of orbital period. In the process, we have also been able to reconstruct a model of the detection efficiency of the global *Kepler* pipeline, and learn about the incidence of false positives of different kinds. We have made an effort to use assumptions in our simulations that we consider to be more realistic than those used in earlier studies of false positives such as that of Morton & Johnson (2011). For convenience we have classified planets into five categories by size: giant planets (6–22 R_{\oplus}), large Neptunes (4–6 R_{\oplus}), small Neptunes (2–4 R_{\oplus}), super-Earths (1.25–2 R_{\oplus}), and Earths (0.8–1.25 R_{\oplus}). The main results may be summarized as follows.

1. We infer the rate of false positives in the *Kepler* field for each planet class, broken down by the type of configuration of the blend (Table 1). This includes eclipsing binaries or other stars transited by larger planets, either of which may be in the background or physically associated with the target. The dominant type of false positive for all planet classes is physically associated stars transited by a larger planet. The overall false positive rate is 17.7% for giant planets, decreasing to a minimum of 6.7% for small Neptunes, and increasing again up to 12.3% for Earth-size planets. On average the mean false positive rate for planets of all sizes is $9.4\% \pm 0.9\%$, which may be compared with the value of 4% derived by MJ11. The difference is due in part to our inclusion of planets transiting companion stars as blends, but other factors listed in Section 1 also have a significant impact.
2. We derive the occurrence rate of planets of different sizes as a function of their orbital period. These results are presented in two different forms: in terms of the average number of planets per star (Table 2 for different period bins, and

cumulative rates in Table 3), and also expressed as the percentage of stars with at least one planet (Table 4). For planets larger than $2 R_{\oplus}$ and periods up to 50 days we may compare our occurrence rates with those of Howard et al. (2012), which are also based on *Kepler* candidates. Our results indicate a rate of 0.209 ± 0.013 planets per star, which is slightly larger than their estimate of 0.166 ± 0.009 . The excess is due to the previously mentioned differences between our approaches. In particular, our prescription for the actual detection recovery rate of *Kepler* (see Section 5.1) leads to a larger occurrence of small Neptunes. For Earth-size planets we find that about 16.5% of stars have at least one planet in this category with orbital periods up to 85 days, beyond which the statistics are still too poor to provide results. Rates for other planet sizes are given in Table 4. The percentage of stars that have at least one planet of any size out to 85 days is approximately 52%. This high percentage is broadly in agreement with results from the HARPS RV survey of Mayor et al. (2011). Those authors reported that the rate of low-mass planets (having masses between 1 and $30 M_{\oplus}$) with periods shorter than 100 days is larger than 50%. While the figures are similar, we must keep in mind that they refer to two different planet properties (radii and masses). A relevant improvement of our procedures we plan for the future is to incorporate a model of the global mass–radius distribution of close-in planets that would simultaneously enable a good match to the mass distribution from Doppler surveys and the radius distribution from *Kepler*.

3. We find that the effective detection efficiency of *Kepler* differs from that expected from the nominal signal-to-noise criterion applied during the mission, namely, that 50% of signals with S/N greater than 7.1 are detectable. Instead, we find that the actual distribution of S/Ns for the KOIs released by Batalha et al. (2013) is better represented with a detection efficiency that increases linearly from 0% for an S/N of 6 to 100% for an S/N of 16.
4. After accounting for false positives and the effective detection efficiency of *Kepler* as described above, we find no significant dependence of the rates of occurrence as a function of the spectral type (or mass, or temperature) of the host star. This contrasts with the findings by Howard et al. (2012), who found that for the small Neptunes ($2\text{--}4 R_{\oplus}$) M stars have higher planet frequencies than F stars.
5. We find an apparent excess of transits of very short duration (less than one hour). Such transits have not explicitly been looked for in the *Kepler* pipeline.

The planet occurrence rates provided in Table 2 should be useful in future planet validation studies (e.g., using the BLENDER procedure) to estimate the “planet prior” (a priori chance of a planet) for a candidate of a given size and period. A comparison of this prior with the a priori chance that the candidate is a false positive, incorporating constraints from any available follow-up observations, could then be used to establish the confidence level of the validation.

Our technique provides an estimate of the occurrence of planets orbiting dwarf stars in the solar neighborhood that is based almost entirely on *Kepler* observations and modeling. Improvements in the *Kepler* pipeline, in the understanding of the detection efficiency and with the addition of more quarters of data, will allow us to improve the planet occurrence estimates, extend them to longer periods, and study their relations with their host stars characteristics.

We thank the anonymous referee for helpful suggestions on the original manuscript. G.T. acknowledges partial support for this work from NASA Grant NNX12AC75G (Kepler Participating Scientist Program).

Facility: *Kepler*

APPENDIX

MODELING OF THE TRANSIT S/N AND OF THE *KEPLER* PHOTOCENTROID SHIFT

A.1. Signal-to-Noise Calculation

In this work, we have adopted the use of the CDPP, which is an empirical measure of the effective noise seen by transits as a function of their duration (Jenkins et al. 2010b; Christiansen et al. 2012). The CDPP is obtained as a time series for each star for each of 14 trial transit durations ranging from 1.5 hr to 15 hr as a by-product of the search for transiting planets by the Kepler Transiting Planet Search (TPS) pipeline. TPS characterizes the power spectral density of each observed flux time series and calculates the expected S/N of the reference transit pulse at each time step. The CDPP time series are obtained by dividing the reference transit depth by the S/N time series, thereby allowing the S/N to be calculated easily for any depth transit of the given duration. We use the rms CDPP calculated across each quarter of *Kepler* observations, and take the median value for each star across Q1 through Q6, interpolating across the 14 CDPP transit durations to estimate the CDPP for each simulated transit or false positive eclipse duration.

The measured CDPP is empirical and accounts for the three known sources of noise: Poisson errors from the number of photons received, which depends on star brightness, the stellar variability noise due to stellar surface physics including spots, turbulence (e.g., granulation), acoustic *p*-modes and magnetic effects, and the residual instrumental effects.

The signal-to-noise ratio of a transit is defined as

$$S/N = \frac{\delta}{CDPP_{\text{eff}}} \sqrt{\frac{t_{\text{obs}} f}{P}}, \quad (\text{A1})$$

where δ is the photometric depth of the signal and is computed as $\delta = R_p^2/R_{\star}^2$ for a transiting planet of radius R_p transiting a star of radius R_{\star} , or as

$$\delta = \frac{R_{\text{ecl}}^2}{R_{\text{blend}}^2} \frac{F_{\text{blend}}}{F_{\text{blend}} + F_{\text{KIC}}} \quad (\text{A2})$$

for a blend involving an object eclipsing a blending star in the photometric aperture of the KIC target. In the above expression, $F_{\text{blend}}/(F_{\text{blend}} + F_{\text{KIC}})$ is the contribution in the *Kepler* bandpass of the flux of the blending star in the photometric aperture normalized to the sum of the blending star and KIC target fluxes. The symbol t_{obs} is the duration of the *Kepler* observations from Q1 to Q6, f is target-specific fraction of the total time the target was observed, and P is the orbital period of the transiting object. The transit duration depends on the mass, size, and period of the eclipsing object, all of which are known from our simulations. Assumptions on the eccentricity have some impact on the S/N through the duration. However, the duration enters only as the square root, so any errors are reduced by a factor of two.

A.2. Centroid Shift Constraint

The most useful observational constraint available to rule out false positives that does not require additional observations is

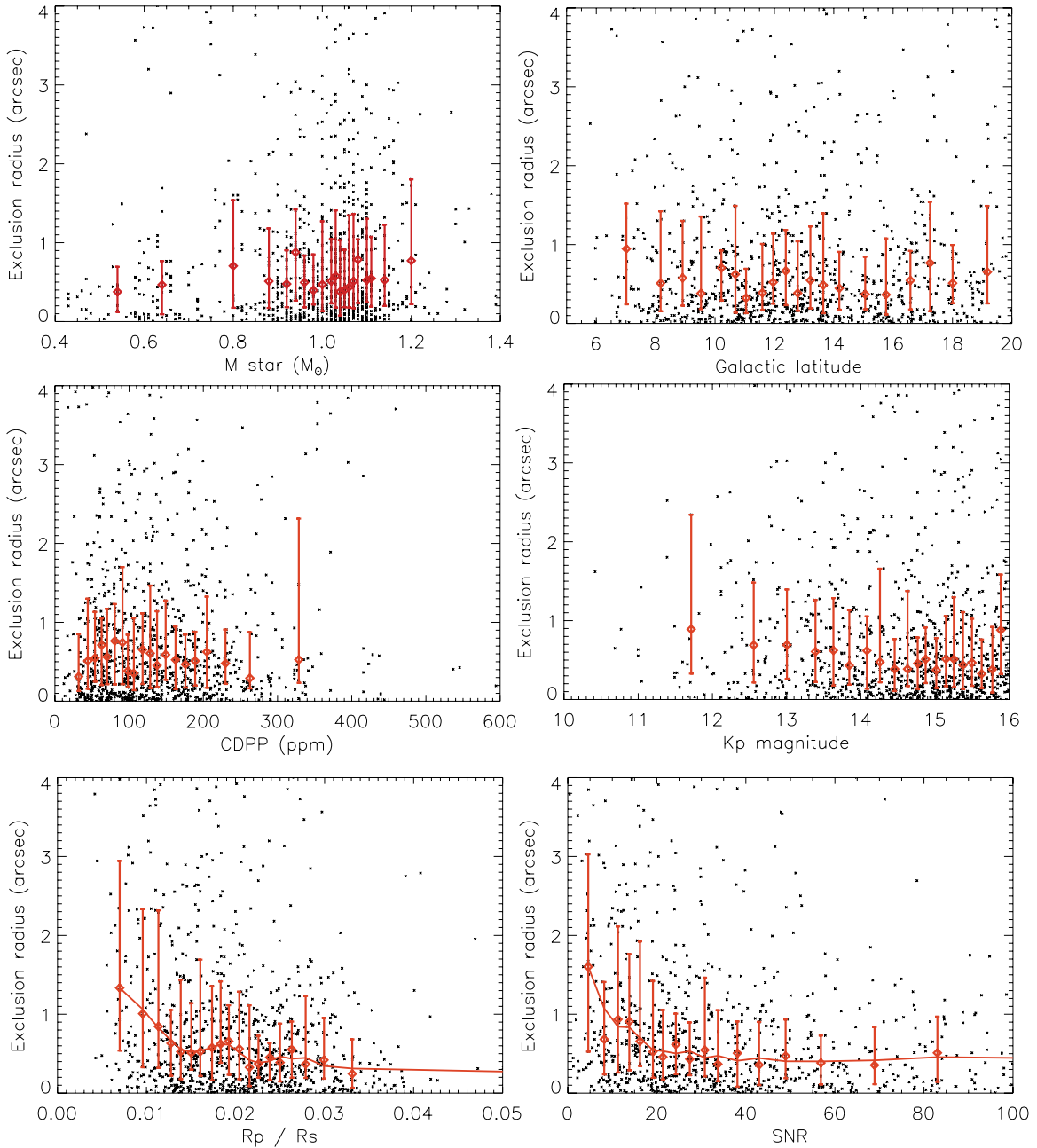


Figure 12. Distribution of the centroid exclusion radius for the 1023 KOIs for which a multi-quarter centroid analysis is available. Black dots are the individual values for the 1023 KOIs. The red diamonds are the median values for bins of 50 KOIs ranked as a function of parameter represented on the horizontal axis. The error bars correspond to the 25 and 75 percentiles. The centroid exclusion radius shows no significant correlation with the spectral type (stellar mass), Galactic latitude, noise level (CDPP), or Kp magnitude of the KOIs. The only significant correlation is with the radius ratio (R_p/R_*) and the transit S/N (which is correlated with R_p/R_*). The red line shows the sliding median of the centroid exclusion radius as a function of these two parameters.

(A color version of this figure is available in the online journal.)

obtained by measuring the photocenter displacement during the transit. If the transit signal is due to a diluted eclipse of another star in the same photometric aperture as the target, there will generally be a shift in the position of the photocenter that occurs during the transit, as the neighboring star contributes less of the total flux at those times.

Of the ~ 2300 KOIs in the cumulative catalog by Batalha et al. (2013), the 1023 new ones that were added to the prior list from Borucki et al. (2011) were subjected to a multi-quarter centroid motion analysis by the *Kepler* team. This analysis

provides a maximum angular separation that corresponds to a 3σ limit beyond which a false positive would have been identified.

In their study, Morton & Johnson (2011) assumed that this exclusion radius scales linearly with the flux from the star and the transit depth, with a lower limit they set at $2''$ and an upper limit at $6''.4$. The sample of 1023 new KOIs with multi-quarter centroid analysis enables us to re-examine the model of MJ11, and test the strength of the proposed correlations between the centroid exclusion radius and those

two parameters (stellar magnitude and transit depth). We also studied the dependencies of the centroid exclusion radius with several other characteristics related to the star and the transit detection.

1. *Spectral type.* By virtue of their different ages, levels of activity, and rotation periods, stars of different spectral types may show different noise patterns that can impact the centroid exclusion radius.
2. *Galactic latitude.* *Kepler* targets located closer to the Galactic plane are likely to have more contamination from background stars in their aperture, which could directly impact the centroid exclusion radius.
3. *Noise level.* We investigated whether the centroid exclusion radius is correlated with the CDPP of each KOI.
4. *Transit signal-to-noise ratio.* As described in the first part of this [Appendix](#), this parameter is correlated with both the CDPP and the transit depth, along with the number of transits and the transit duration.

For this paper we require a prescription for predicting the approximate multi-quarter centroid exclusion radius for each *Kepler* target to be used in our simulations. It is sufficient for our purposes to be able to predict a reasonable *range* for this quantity. Figure 12 shows that the centroid exclusion radius has a large scatter, regardless of which parameter we display it against. Median values in appropriate bins do not appear to show any correlation with the spectral type (or equivalently stellar mass M_*), Galactic latitude, or the CDPP. The centroid exclusion radius shows only a weak correlation with the *Kepler* magnitude, but different from the linear correlation with the flux proposed by MJ11: there is little variation except for the faintest bin ($Kp > 15.8$ mag), which is likely due to the higher background noise level, and for the brightest stars ($Kp < 12$ mag), due to the fact that *Kepler* stars saturate below a magnitude of about 11.5 (Batalha et al. 2013). The clearest correlation in the centroid exclusion radius is with the transit depth $(R_p/R_*)^2$ (with a Pearson correlation coefficient of -0.1), and with the transit S/N (with a Pearson correlation coefficient of -0.08), which is of course highly correlated with the transit depth (Equation (A1)).

In order to make use of this correlation with the transit S/N for our simulations, and at the same time to account for the large scatter present in that correlation, we proceeded as follows. We first computed the S/N of each false positive scenario we simulated using Equation (A1), and we then selected a random exclusion radius from the sub-sample of the 1023 KOIs having an S/N within 10% of the one of this false positive. This is the

exclusion radius we used for our emulation of the *Kepler* vetting procedure.

REFERENCES

- Ballard, S., Fabrycky, D., Fressin, F., et al. 2011, [ApJ](#), **743**, 200
- Batalha, N. M., Borucki, W. J., Bryson, S. T., et al. 2011, [ApJ](#), **729**, 27
- Batalha, N. M., Rowe, J. F., Bryson, S. T., et al. 2013, [ApJS](#), **204**, 24
- Borucki, W. J., Koch, D. G., Basri, G., et al. 2011, [ApJ](#), **736**, 19
- Borucki, W. J., Koch, D. G., Batalha, N., et al. 2012, [ApJ](#), **745**, 120
- Bowler, B. P., Johnson, J. A., Marcy, G. W., et al. 2010, [ApJ](#), **709**, 396
- Brown, T. M. 2003, [ApJL](#), **593**, L125
- Brown, T. M., Latham, D. W., Everett, M. E., & Esquerdo, G. A. 2011, [AJ](#), **142**, 112
- Burke, C. J., Christiansen, J. L., Jenkins, J. M., et al. 2012, [BAAS](#), **219**, 245.07
- Catanzarite, J., & Shao, M. 2011, [ApJ](#), **738**, 151
- Christiansen, J. L., Jenkins, J. M., Barclay, T. S., et al. 2012, [PASP](#), **124**, 1279
- Cochran, W. D., Fabrycky, D. C., Torres, G., et al. 2011, [ApJS](#), **197**, 7
- Demory, B.-O., & Seager, S. 2011, [ApJS](#), **197**, 12
- Dressing, C., & Charbonneau, D. 2013, [arXiv:1302.1647](#)
- Farmer, A. J., & Agol, E. 2003, [ApJ](#), **592**, 1151
- Fressin, F., Torres, G., Désert, J.-M., et al. 2011, [ApJS](#), **197**, 5
- Fressin, F., Torres, G., Pont, F., et al. 2012a, [ApJ](#), **745**, 81
- Fressin, F., Torres, G., Rowe, J. F., et al. 2012b, [Natur](#), **482**, 195
- Gautier, T. N., III, Charbonneau, D., Rowe, J. F., et al. 2012, [ApJ](#), **749**, 15
- Girardi, L., Bressan, A., Bertelli, G., & Chiosi, C. 2000, [A&AS](#), **141**, 371
- Girardi, L., Groenewegen, M. A. T., Hatziminaoglou, E., & da Costa, L. 2005, [A&A](#), **436**, 895
- Holman, M. J., & Wiegert, P. A. 1999, [AJ](#), **117**, 621
- Howard, A. W., Marcy, G. W., Bryson, S. T., et al. 2012, [ApJS](#), **201**, 15
- Jenkins, J. M., Caldwell, D. A., Chandrasekaran, H., et al. 2010a, [ApJL](#), **713**, L87
- Jenkins, J. M., Chandrasekaran, H., McCauliff, S. D., et al. 2010b, [Proc. SPIE](#), **7740**, 77400D
- Jenkins, J. M., Doyle, L. R., & Cullers, D. K. 1996, [Icar](#), **119**, 244
- Johnson, J. A., Aller, K. M., Howard, A. W., & Crepp, J. R. 2010, [PASP](#), **122**, 905
- Latham, D. W., Bakos, G. Á., Torres, G., et al. 2009, [ApJ](#), **704**, 1107
- Lissauer, J. J., Marcy, G. W., Rowe, J. F., et al. 2012, [ApJ](#), **750**, 112
- Mann, A. W., Gaidos, E., Lépine, S., & Hilton, E. J. 2012, [ApJ](#), **753**, 90
- Mayor, M., Marmier, M., Lovis, C., et al. 2011, [arXiv:1109.2497](#)
- Moorhead, A. V., Ford, E. B., Morehead, R. C., et al. 2011, [ApJS](#), **197**, 1
- Morton, T. D. 2012, [ApJ](#), **761**, 6
- Morton, T. D., & Johnson, J. A. 2011, [ApJ](#), **738**, 170
- Muirhead, P. S., Hamren, K., Schlawin, E., et al. 2012, [ApJL](#), **750**, L37
- Pinsonneault, M. H., An, D., Molenda-Zakowicz, J., et al. 2012, [ApJS](#), **199**, 30
- Pont, F., Zucker, S., & Queloz, D. 2006, [MNRAS](#), **373**, 231
- Prša, A., Batalha, N., Slawson, R. W., et al. 2011, [AJ](#), **141**, 83
- Raghavan, D., McAlister, H. A., Henry, T. J., et al. 2010, [ApJS](#), **190**, 1
- Robin, A. C., Reylé, C., Derrière, S., & Picaud, S. 2003, [A&A](#), **409**, 523
- Santerne, A., Díaz, R. F., Moutou, C., et al. 2012, [A&A](#), **545**, A76
- Slawson, R. W., Prša, A., Welsh, W. F., et al. 2011, [AJ](#), **142**, 160
- Torres, G., Fressin, F., Batalha, N. M., et al. 2011, [ApJ](#), **727**, 24
- Torres, G., Konacki, M., Sasselov, D. D., & Jha, S. 2004, [ApJ](#), **614**, 979
- Traub, W. A. 2012, [ApJ](#), **745**, 20
- Youdin, A. N. 2011, [ApJ](#), **742**, 38